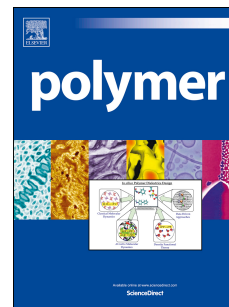


Accepted Manuscript

New Bead Type and High Symmetrical Diallyl-POSS Based Emissive Conjugated Polyfluorene

Jin Huang, Weina Wang, Jiangjing Gu, Weizhi Li, Qihong Zhang, Yin Ding, Kai Xi, Youxuan Zheng, Xudong Jia



PII: S0032-3861(14)01004-0

DOI: [10.1016/j.polymer.2014.10.071](https://doi.org/10.1016/j.polymer.2014.10.071)

Reference: JPOL 17388

To appear in: *Polymer*

Received Date: 6 July 2014

Revised Date: 13 October 2014

Accepted Date: 30 October 2014

Please cite this article as: Huang J, Wang W, Gu J, Li W, Zhang Q, Ding Y, Xi K, Zheng Y, Jia X, New Bead Type and High Symmetrical Diallyl-POSS Based Emissive Conjugated Polyfluorene, *Polymer* (2014), doi: 10.1016/j.polymer.2014.10.071.

This is a PDF file of an unedited manuscript that has been accepted for publication. As a service to our customers we are providing this early version of the manuscript. The manuscript will undergo copyediting, typesetting, and review of the resulting proof before it is published in its final form. Please note that during the production process errors may be discovered which could affect the content, and all legal disclaimers that apply to the journal pertain.

New Bead Type and High Symmetrical Diallyl-POSS Based Emissive Conjugated Polyfluorene

Jin Huang,^{a,b} Weina Wang,^{a,b} Jiangjing Gu,^{a,b} Weizhi Li,^{a,b} Qihong Zhang,^{a,b} Yin Ding,^c Kai Xi,^b

Youxuan Zheng,^a Xudong Jia^{*a,b}

^aState Key Laboratory of Coordination Chemistry, Nanjing National Laboratory of Microstructures, Nanjing University, Nanjing 210093, PR China

^bDepartment of Polymer Science & Engineering, Nanjing University, Nanjing 210093, PR China

^cState Key Laboratory of Analytical Chemistry for Life Science, Nanjing University, Nanjing 210093, PR China

ABSTRACT: A new bead type and diallyl-POSS based polyfluorene (**P2**) with high symmetrical structure was synthesized via Heck coupling reaction between oligomeric alkynyl fluorene (**P1**) and diallyl polyhedral oligomeric silsesquioxanes (diallyl-POSS). The molecular weight and the conjugated length of **P1** and **P2** were well controlled to acquire good solubility and excellent optical property. The bead-type POSS based polymer was characterized by gel permeation chromatography (GPC), FT-IR, ¹H NMR and photoluminescence (PL) spectra. High Resolution Transmission Electron Microscopy (HRTEM) micrographs showed that diallyl-POSS were uniformly nano-dispersed in the polymer matrix. Compared with **P1**, the POSS-based polyfluorene **P2** exhibited not only a higher thermal stability, but also an improved photophysical property in solution and solid states. The incorporation of diallyl-POSS resulted effectively in inhibiting the strong stacking/dipole–dipole interaction between fluorescent groups in the polyfluorene. The experimental results indicate that the bi-functional POSS based light-emitting polymers with high symmetrical structure can have great potential in optical materials and devices, such as OPV or PLED, etc.

Keywords: Diallyl-POSS, polyfluorene, light-emitting polymer.

1. Introduction

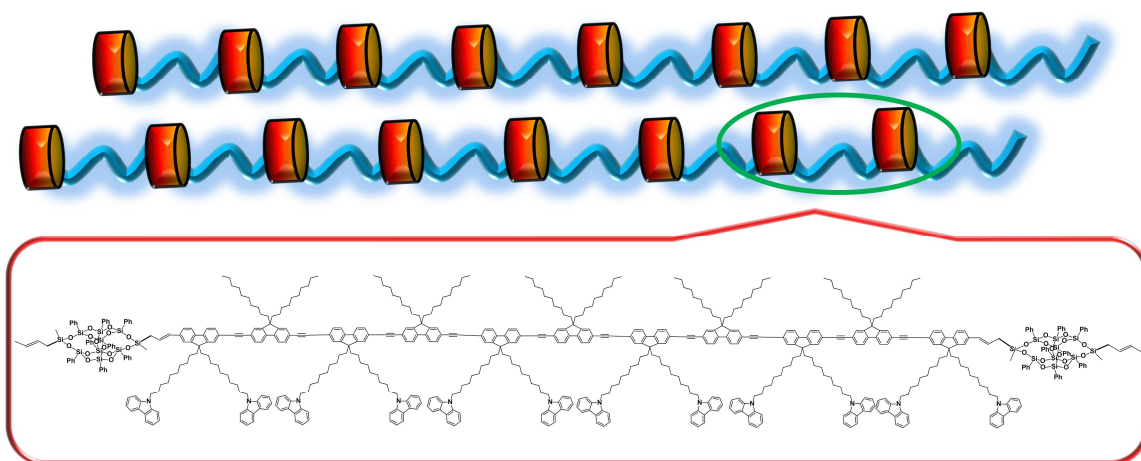
* Corresponding authors. Tel: +86-25-83593041; Fax: +86-25-83621337.

E-mail addresses: jiaxd@nju.edu.cn (X. D. Jia).

Semiconductor light-emitting polymers have attracted extensive attention on account of their great application prospect in the fields of organic photovoltage (OPV) [1], polymer light-emitting diode (PLED) [2], biological imaging [3], photodynamic therapy [4], sensing [5], etc. In recent years, semiconductor light-emitting polymers containing polyfluorene structure have been a hotspot because of their high fluorescence efficiency [6], excellent two-photon fluorescence property [7], remarkable chemical/thermal stability [8], and extraordinary electronic transmission property [9]. However, serious fluorescence quenching exists, which is attributed to a strong dipole–dipole and π – π stacking interaction between the chromophores [10]. Furthermore, the emission spectra of polyfluorene materials always exhibit shoulder peaks around 530 nm, which affects the emission color purity. In view of this, the application of polyfluorene in luminescent material has been hindered [11].

To break these bottle-necks, one approach is to introduce POSS into polyfluorene optical materials [12]. It is known that the incorporation of a particular cage structure consisting of inorganic Si-O core can improve the thermal stability and photo-stability [13]. Additionally, the appropriate numbers of external organic groups of POSS with good symmetry could avoid functional groups lying in closer proximity to each other, which would reduce the opportunity for self-absorption thus enhance fluorescence quantum yield [14]. So far, copious cross-linked structures [15], pendent-type [16], star-type [17] POSS-based polyfluorene polymers have been synthesized to overcome the formation of aggregation or keto defect in polyfluorenes.

Recently, Laine et al. have studied the photophysical properties of T_8 (octahedral POSS), T_{10} (decahedral POSS) and T_{12} (dodecahedral POSS) with *p*-vinylstilbene structure and found that the size of Si-O cage and the symmetry of the structure can significantly impact on fluorescence quantum yield [18]. More importantly, the incorporation of POSS with symmetrical structure greatly enhances the two-photon fluorescence (TPF) and two-photon absorption (TPA) cross section on account of very rigid Si-O cage.



Scheme 1. Construction of diallyl-POSS bridged organic-inorganic luminescent polyfluorene.

However, few researches have been reported about bead-type POSS-based light-emitting polymers. In this article, diallyl-POSS (T_8D_2 type) with highly symmetrical structure was synthesized, and a diallyl-POSS-based hybrid polymer with bead type structure was then prepared (Scheme 1). Meanwhile, the conjugation length of oligomeric alkynyl fluorene structure between the adjacent diallyl-POSS, which was nailed on the main chain of polymer via Heck cross-coupling reactions, was well controlled in order to acquire excellent luminescent properties and solubility. The incorporation of “huge” inorganic POSS nanoparticles to form bead type and high symmetrical diallyl-POSS based polymer molecular chain was expected to improve not only the thermal property of light-emitting polymer, but also the optical properties including a higher fluorescent quantum yield, enhanced photo-stability and much improved two-photon fluorescence (TPF) property. It is expected that bifunctional-POSS based polymer will have great impact on applications in optical materials and devices, such as OPV or PLED, etc.

2. Experimental Section

2.1. Materials

1-Bromodecane (98%), 2,7-dibromofluorene (98%), tetrabutyl ammoniumbromide (98%), carbazole (98%), bis(triphenylphosphine) palladium (II) chloride (98%) purchased from Nanjing Carbon Reagent Co. Ltd. Cuprous iodide (99%), 2-methylbut-3-yn-2-ol (98%), 1,10-dibromodecane (98%), sodium hydroxide and anhydrous potassium carbonate (98%) were used as received from Adamas. Allyl(dichloro)methylsilane (95%) was obtained from TCI

(Shanghai) Chemical Industry Development Co., Ltd. Tetrasilanolphenyl POSS was purchased from Hybrid Plastics. All organic solvents were purchased from commercial sources and were carefully dried and distilled prior to use.

2.2. The synthesis of monomers and polymers

2.2.1. *2,7-dibromo-9,9-didecylfluorene (1)*. 1-Bromodecane (4.42 g, 20.0 mmol) was added by syringe to a mixture of 2,7-dibromofluorene (2.59 g, 8 mmol), tetrabutyl ammonium bromide (0.02 g, 0.064 mmol) and 2.50 mL of 50% aqueous sodium hydroxide in dimethyl sulfoxide (50.0 mL). After stirring at room temperature for 4 h, the mixture was poured into water and extracted three times with dichloromethane. The solvent was removed under reduced pressure and the precipitate was purified by column chromatography on silica gel (eluent: petroleum ether) to afford 2,7-dibromo-9,9-didecylfluorene as a white powder (4.45 g, Yield 92%). ¹H NMR (500 MHz, CDCl₃, δ): 7.51 (d, 2H, *J* = 8.70 Hz, Ar-H), 7.45 (m, 4H, Ar-H), 1.91 (m, 4H, CH₂), 1.13 (m, 28H, CH₂), 0.85 (t, 6H, *J* = 6.95 Hz, CH₃), 0.58 (m, 4H, CH₂). FT-IR (cm⁻¹, KBr): ν = 2950, 2836 (s; CH), 1638, 1551 (w; Ar). Anal. Calcd. for C₃₃H₄₈Br₂: C 65.56, H 8.00; Found: C 64.72, H 7.62.

2.2.2. *4,4'-(9,9-didecyl-9H-fluorene-2,7-diyl)bis(2-methylbut-3-yn-2-ol) (2)*. Under argon atmosphere, 2,7-dibromo-9,9-didecylfluorene (1.21 g, 2 mmol), 2-methylbut-3-yn-2-ol (1.6 mL, 16 mmol), bis(triphenylphosphine) palladium(II) chloride (24 mg, 0.08 mmol) and cuprous iodide (8 mg, 0.04 mmol) were dissolved in 20 mL of triethylamine and 40 mL of tetrahydrofuran. The mixture was refluxed at 70 °C for 24 h. After cooling to room temperature, the insoluble substance was filtered off. Then the solvent was removed under reduced pressure. The mixture was extracted three times with dichloromethane. The organic phase was purified by column chromatography on silica gel with ethyl acetate/petroleum ether (1:8 v/v) to afford 4,4'-(9,9-didecyl-9H-fluorene-2,7-diyl)bis(2-methylbut-3-yn-2-ol) as a yellow powder (0.87 g, Yield 71%). ¹H NMR (500 MHz, CDCl₃, δ): 7.59 (d, *J* = 7.9 Hz, 2 H, Ar-H), 7.39 (m, 4 H, Ar-H), 1.92 (m, 4H, CH₂), 1.66 (s, 12H, CH₃), 1.28–1.02 (m, 28H, CH₂), 0.85 (t, *J* = 7.15 Hz, 6 H), 0.54 (m, 4H, CH₂). FT-IR (cm⁻¹, KBr): 3330 (m; OH), 2927, 2856 (s; CH), 2220 (w; C≡C), 1622, 1541 (w; Ar). Anal. Calcd. For C₄₃H₆₂O₂: C, 84.39; H, 10.20. Found: C, 84.53; H, 10.23.

2.2.3. *9,9-didecyl-2,7-diethynylfluorene (3)*. Under argon atmosphere,

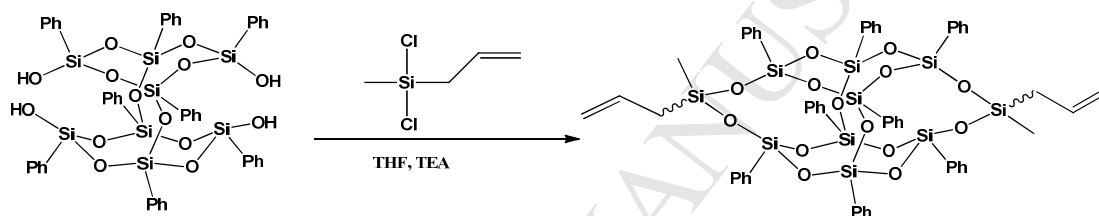
4,4'-(9,9-didecyl-9*H*-fluorene-2,7-diyl)bis(2-methylbut-3-yn-2-ol) (0.61 g, 1 mmol) and sodium hydroxide (0.60 g, 10 mmol) in 40 mL of 1,4-dioxane were refluxed at 80 °C for 6 h. After cooling to room temperature, water and dichloromethane were added to the mixture, and the organic phase purified by column chromatography on silica gel with petroleum to get 9,9-didecyl-2,7-diethynylfluorene as white crystals (0.46 g, Yield 92%). ¹H NMR (500 MHz, CDCl₃, δ): 7.62 (d, *J* = 8.0 Hz, 2 H, Ar-H), 7.46 (m, 4 H, Ar-H), 3.13 (s, 2 H, C≡C-H), 1.93 (m, 4 H, CH₂), 1.25–1.02 (m, 28H, CH₂), 0.85 (t, *J* = 7.2 Hz, 6 H, CH₃), 0.56 (m, 4H, CH₂). ¹³C NMR (500 MHz, CDCl₃, δ): 151.04, 141.02, 131.35, 126.56, 121.07, 119.94, 84.54, 77.47, 55.27, 40.30, 31.98, 30.03, 29.83, 29.63, 29.35, 29.31, 23.73, 22.72, 14.19. FT-IR (cm⁻¹, KBr): 3310 (s; C≡C-H), 2924, 2850 (s; CH), 2100 (w; C≡C), 1638, 1573 (m; Ar). Anal. Calcd. For C₃₇H₅₀: C, 89.81; H, 10.19. Found: C, 89.67; H, 10.23.

2.2.4. 9-(10-bromodecyl)-9*H*-carbazole (**4**). Under argon atmosphere, carbazole (1.67 g, 0.01 mol), anhydrous potassium carbonate (2.77 g, 0.02 mol), and 1,10-dibromodecane (6.00 g, 0.02 mol) in 40 mL of anhydrous acetonitrile were refluxed at 95 °C for 36 h. After cooling to room temperature, insoluble substance was filtered, and the solvent was removed under reduced pressure. The crude product was purified by column chromatography on silica gel with petroleum to get 9-(10-bromodecyl)-9*H*-carbazole as white crystals (1.66 g, Yield 43%). ¹H NMR (500 MHz, CDCl₃, δ): 8.08 (d, *J* = 7.7 Hz, 2 H, Ar-H), 7.43 (t, *J* = 7.8 Hz, 2 H, Ar-H), 7.35 (d, *J* = 8.1 Hz, 2 H, Ar-H), 7.20 (t, *J* = 7.5 Hz, 2 H, Ar-H), 4.21 (t, *J* = 7.3 Hz, 2 H, CH₂), 3.33 (t, *J* = 6.8 Hz, 2 H, CH₂Br), 1.79 (m, 4 H, CH₂), 1.33–0.91 (m, 12 H, CH₂). FT-IR (cm⁻¹, KBr): 2930, 2850 (s; CH), 1632, 1619, 1593 (m; Ar). Anal. Calcd. For C₂₂H₂₈BrN: C, 68.39; H, 7.30; N, 3.63; Found: C, 68.47; H, 7.25; N, 3.56.

2.2.5. 9,9'-((2,7-dibromo-9*H*-fluorene-9,9-diyl)bis(decane-10,1-diyl))bis(9*H*-carbazole) (**5**). 9-(10-bromodecyl)-9*H*-carbazole (1.55 g, 4 mmol) was added by syringe to a mixture of 2,7-dibromofluorene (0.32 g, 1 mmol), tetrabutyl ammonium bromide (3 mg, 0.008 mmol) and 0.313 mL of 50% aqueous sodium hydroxide dissolved in dimethyl sulfoxide (10.0 mL). After stirring at 40°C for 6 h, the mixture was poured into water and extracted three times with dichloromethane. The solvent was removed under reduced pressure. The precipitate was purified by column chromatography on silica gel ethyl acetate/petroleum (1:20 v/v) to afford 9,9'-((2,7-dibromo-9*H*-fluorene-9,9-diyl)bis(decane-10,1-diyl))bis(9*H*-carbazole) as white

crystals (0.36 g, Yield 38%). ^1H NMR (500 MHz, CDCl_3 , δ): 8.08 (d, $J = 7.5$ Hz, 4 H, Ar-H), 7.46 (m, 14 H, Ar-H), 7.21 (d, $J = 7.4$ Hz, 4 H, Ar-H), 4.25 (t, $J = 7.6$ Hz, 4 H, CH_2), 1.89–1.78 (m, 8 H, CH_2), 1.31–0.95 (m, 24 H, CH_2), 0.53 (m, 4 H, CH_2). ^{13}C NMR (500 MHz, CDCl_3 , δ): 152.56, 140.45, 139.11, 130.21, 126.19, 125.61, 122.86, 121.52, 121.20, 120.38, 118.72, 108.69, 55.73, 43.09, 40.16, 29.79, 29.41, 29.38, 29.36, 29.10, 28.97, 27.32, 23.62. FT-IR (cm^{-1} , KBr): 2936, 2861 (s; CH), 1636, 1621, 1582 (m; Ar). Anal. Calcd. For $\text{C}_{57}\text{H}_{62}\text{Br}_2\text{N}_2$: C, 73.23; H, 6.68; N, 3.00; Found: C, 73.34; H, 6.82; N, 2.93.

2.2.6. 3,13-di(3-propenyl)-3,13-dimethyl-1,5,7,9,11,15,17,19-octaphenylhexacyclo [15.3.1(1,13).1(3,11).1(5,17).1(9,15)]decasiloxane (**6**). **6** was synthesized according to the pathway shown in Scheme 2:



Scheme 2. Synthesis of 3,13-di(3-propenyl)-3,13-dimethyl-1,5,7,9,11,15,17,19-octaphenylhexacyclo [15.3.1(1,13).1(3,11).1(5,17).1(9,15)]decasiloxane.

Under dry argon atmosphere, allyl(dichloro)methylsilane (3.102 g, 1.46 mL, 10 mmol) was added dropwise to a mixed solution of 40 mL of anhydrous tetrahydrofuran, tetrasilanolphenyl POSS (5.350 g, 5 mmol), and triethylamine (0.81 mL, 5 mmol) at room temperature. After 30 minutes, the insoluble solid was filtered off and the solvent and other volatile compounds were removed under reduced pressure. The crude product was washed with 50 mL of methanol, 5 mL of ether and 2 mL of hydrochloric acid (1 mol/L) to afford *cis*- and *trans*-**6** as a white powder (3.89 g, Yield 63%). *Cis*- and *trans*-**6** (in the presence of isomeric mixture of 1:1 ratio): ^1H NMR (500 MHz, CDCl_3 , δ): 7.53–7.19 (m, 40 H, Ar-H), 5.76 (m, 2 H, $\text{CH}=\text{CH}_2$), 4.88–4.76 (m, 4 H, $\text{CH}=\text{CH}_2$), 1.77 (d, 4 H, $J = 7.8$ Hz, CH_2), 0.30 (s, 6 H, CH_3 , indicated isomeric mixture). ^{29}Si NMR (500 MHz, CDCl_3 , δ): -21.96, -78.58, -79.49 (*trans*-**6**; relative intensity ratio 1:2:2); -21.96, -78.58, -79.45, -79.53 (*cis*-**6**; relative intensity ratio 1:2:1:1). FT-IR (cm^{-1} , KBr): 1639, 1591 (w; Ar), 1097 (s; Si–O–Si). Anal. Calcd. For $\text{C}_{56}\text{H}_{56}\text{O}_{14}\text{Si}_{10}$: C, 54.51; H, 4.57; Found: C, 54.64; H, 4.73. MALDI-TOF MS [$\text{C}_{56}\text{H}_{56}\text{O}_{14}\text{Si}_{10} + \text{Na}$] $^+$: Calcd. 1256.89, found 1255.25.

2.2.7. *Synthesis of oligomeric alkynyl fluorene (P1)*. 9,9'-((2,7-dibromo-9H-fluorene-9,9-diyl)bis(decane-10,1-diyl))bis(9H-carbazole) (701 mg, 0.75 mmol), 9,9-didecyl-2,7-diethynylfluorene (247 mg, 0.5 mmol), tetrakis(triphenylphosphine) palladium(0) (23 mg, 2 mol %), copper iodide (10 mg, 5 mol %), *N,N*-diisopropylamine (5 mL), and toluene (10 mL) were added into a Schlenk flask in a nitrogen-filled glove box. After stirring at 60 °C for 12 h, the dibromo monomer (**5**) (94 mg, 0.10 mmol) in THF (5 mL) was added from a syringe. After another 12 hours at 60 °C, the polymer was precipitated into methanol, and the solid was filtered and washed in a Soxhlet extractor with methanol followed by acetone to remove residual catalyst and low-molecular-weight material. The crude product was purified by column chromatography on silica gel tetrahydrofuran/hexane (3:1 v/v) to remove high molecular weight material. The yield was 32% as an orange solid. $M_w = 8.79 \times 10^3$ Da, $M_n = 4.61 \times 10^3$ Da, PDI = 1.91, (GPC, polystyrene); FT-IR (cm^{-1} , KBr): 2923, 2852 (CH), 1627, 1604, (Ar); ^1H NMR (500 MHz, CDCl_3 , δ): 8.07 (4H, Ar-H), 7.67–7.38 (20H, Ar-H), 7.21 (4H, Ar-H), 4.26 (4H, N-CH₂), 1.87–0.54 (78H, (CH₂)₁₀ and (CH₂)₁₀CH₃).

2.2.8. *Synthesis of bead-type POSS-based hybrid (P2)*. Bead-type POSS-based hybrid (**P2**) was prepared from oligomeric alkynyl fluorine (**P1**) and diallyl-POSS (molar feed ratio 1:1) through conventional Heck coupling reaction using palladium acetate as a catalyst, anhydrous potassium carbonate as an acid binding agent, and *N,N*-dimethyl glycine (DMG) as a ligand at 120 °C in dry *N*-methyl pyrrolidone. Under dry argon atmosphere, a mixture of **P1** (440 mg, 0.05 mmol), diallyl-POSS (62 mg, 0.05 mmol), DMG (31 mg, 0.3 mmol), palladium acetate (4 mg, 0.015 mmol), anhydrous potassium carbonate (21 mg, 0.015 mmol) and *N*-methyl pyrrolidone (5 ml) were added into a Schlenk flask in a nitrogen-filled glove box and stirred at 120 °C for 20 h. After cooling to room temperature, solvent was removed by vacuum distillation. The polymer was then precipitated into water and filtered, washed in a Soxhlet extractor with acetone/dichloromethane (6:1 v/v). The crude product was purified by column chromatography on silica gel tetrahydrofuran. In this way, the much high molecular weight product could be removed to improve the solubility of **P2**. The yield was 35% as a dark green solid. $M_w = 3.93 \times 10^4$ Da, $M_n = 1.45 \times 10^4$ Da, PDI = 2.71, (GPC, polystyrene); ^1H NMR (500 MHz, CDCl_3 , δ): 8.09 (br, Ar-H), 7.67–7.36 (br, Ar-H), 7.20 (br, Ar-H), 5.45 (br, CH=CH), 4.26 (br, N-CH₂), 1.97–0.60 (br, (CH₂)₁₀ and (CH₂)₁₀CH₃). ^{29}Si NMR (79.49 MHz, solid, δ): -18.12, -65.22, -79.10. FT-IR (cm^{-1} , KBr): 2923, 2852 (CH),

1681, 1663, 1581 (Ar), 1118 (Si–O–Si).

2.3. Preparation Fluorescent Composite Film

8.89 g (0.04 mol) of 3-isocyanatomethyl-3,5,5-trimethylcyclohexyl isocyanate (IPDI), 20 g (0.02 mol) of poly-caprolactone diol (PCL $M_w=1000$) and 50 μ L of dibutyltin dilaurate were added to a three-necked bottle with mechanical agitation, and reacted 6 h at 80 °C. 1.80 g (0.02 mol) of 1,4-butylene glycol (BDO) and 30 ml of THF were added after cooling to room temperature. The mixture was used as matrix solution. 6 mg/ml THF solutions of **P1** and **P2** were prepared respectively, and different volumes of **P1** and **P2** THF solution, according to different mass fractions of **P1** and **P2** in fluorescence composite films, were added to 2 ml of the former matrix solution with magnetic stirring. The mixture was then added to the teflon plate. The solvent was evaporated 24 h at room temperature, and then was placed into an oven at 60 °C for 2 days. Finally, the residue solvent was evaporated under vacuum at 30 °C for 10 h.

2.4. Measurements and Techniques

2.4.1. Molecular Structure Characterizations

Infrared spectra were obtained with a Bruker VECTOR 22 Fourier-transform infrared (FT-IR) spectrometer. The ^1H NMR, ^{13}C HNR and ^{29}Si NMR spectra were recorded in trichloromethane-d using tetramethylsilane as internal standard on a Bruker 500 (500 MHz). The solid ^{29}Si NMR spectrum of P2 was obtained with Bruker AVANCE III (400MHz).

Elemental Analysis data were obtained using a CHN-O-Rapid elemental analyzer (Foss. Heraeus, Germany). Matrix-assisted ultraviolet laser desorption/ionization time of flight mass spectroscopy (MALDI-TOF-MS) of diallyl-POSS monomer was performed using a Bruker Daltonics Autoflex TOF/TOF in linear and reflection modes. Gentsic acid (2,5-dihydroxybenzoic acid, DHB) was used as the matrix with tetrahydrofuran as the solvent. Sodium was used as the cationizing agent.

Molecular weight of polymers was measured on gel permeation chromatography (GPC) apparatus equipped with UV-vis detection and Waters 1515 HPLC pump. Tetrahydrofuran was used as a carrier solvent at a flow rate of 1.0 mL/min at 25 °C. A calibration curve was made to determine M_n and M_w/M_n values with polystyrene standards, $M_w=900\sim 1.74\times 10^6$ g/mol, $D<$

1.1. Simultaneous TG-DTA Netzsch STA 449F3 was used to investigate the thermal stability of the polymers in nitrogen atmosphere from ambient temperature to 700 °C at a heating rate of 10 °C min⁻¹.

2.4.2. Morphological Characterizations

Morphological observations were done by High Resolution Transmission Electron Microscopy (HRTEM). The polymers were embedded by epoxy resin, and ultrathin sections were made by using LeicaULTRACUT UC6 with approximate thickness about 70 nm. The ultrathin sections were then collected onto copper grids. The copper grids were imaged using a JEM-2100 transmission electron microscope at 200 kV.

Surface topography was characterized by atomic force microscopy (AFM) in tapping mode using silicon tips with Olympus OMCL-AC160TS and controller from Veeco Corporation. The sample was spin-coated on silicon wafer surface by THF solutions of P2 films (2 wt %) and cured in a vacuum oven at 334 K for 12 h.

2.4.3. Optical Performance Characterizations

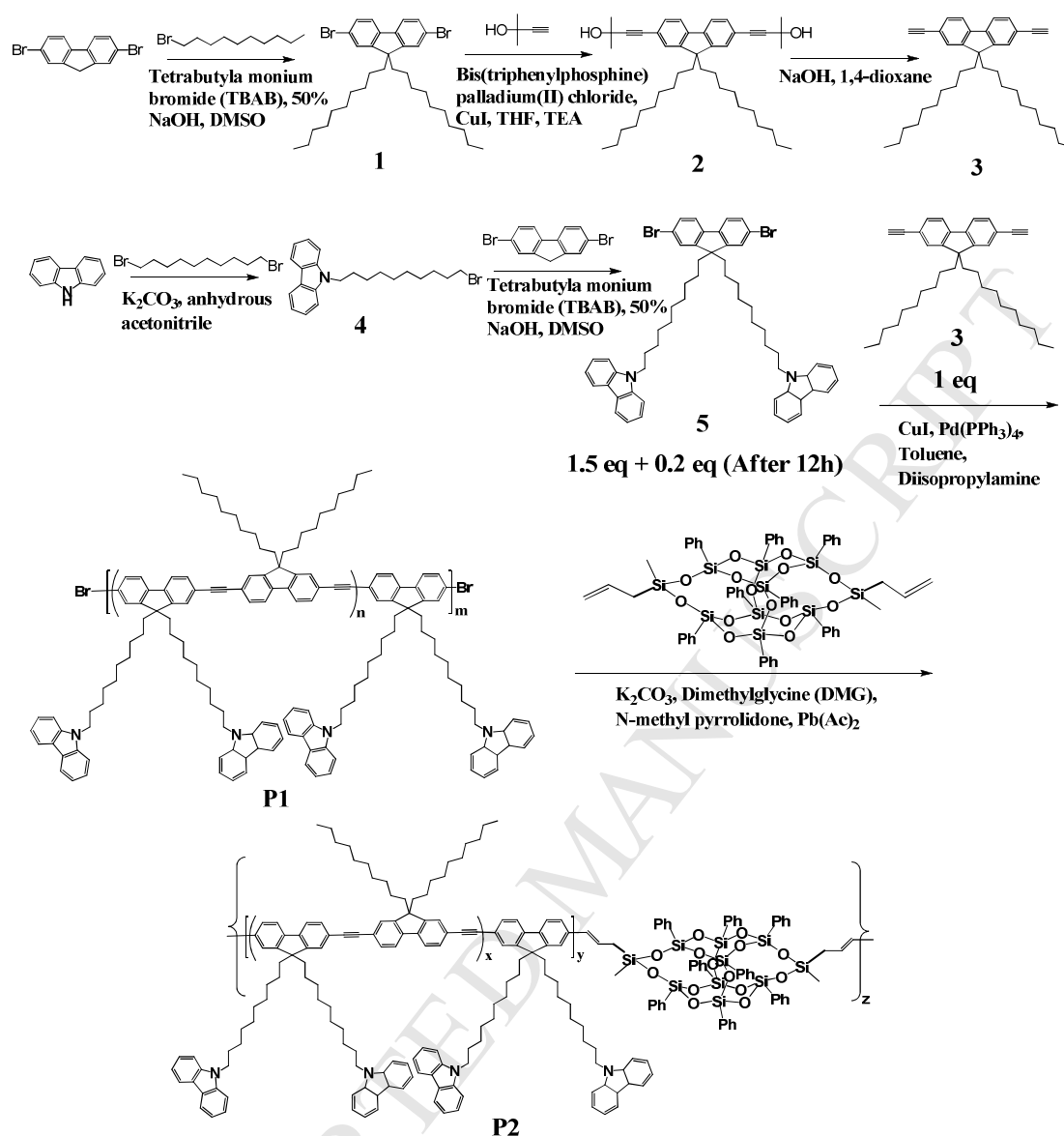
Ultraviolet-visible (UV-vis) absorption of the obtained polymers solution was carried on a UV-1800 (PC) UV-vis spectrophotometer (Mapada, China). The solution fluorescence spectrums of the compound were measured with a FluoroMax-4 spectrofluorometer (HORIBA Scientific, Japan). The solid thin films of polymers were prepared by spinning coating 10 mg/ml polymer solution on the quartz glass plate with a spin rate of 2000 rpm. The solid thin film of polymers and the fluorescent composite films fluorescence spectrums were recorded on a FP-6600 (Jasco Inc.) spectrophotometer using a quartz cell with an optical path length of 1 mm. The photoluminescence QYs were determined on the spectrophotometer with an integrating sphere (ISF-513). TPF spectra of P1 and P2 in dilute solution and TPF imaging of composite films were performed using Leica TCS SP5 laser scanning confocal microscope with a Ti:sapphire laser (Mira Optima 900F, Coherent) as the excitation source. The laser is tuned at 780 nm with 0.5 mW power after the objective and provides ca. 100-fs pulses at a repetition rate of 76 MHz. The details of the two-photon technique experimental setup are described elsewhere [19].

3. Results and Discussion

3.1. Synthesis and Characterization

An appropriate conjugation length and molecular weight are crucial factors to influence the property of solubility and emission for the light-emitting polymer. In this work, the molecular weight and the conjugated length of **P1** were controlled by adding excess amount of monomers **5** step by step in the synthesis procedure, followed by washing repeatedly with acetone to remove small molecules in the purification procedure and using column chromatography to take away high molecular weight polymers to prevent insoluble substance generating in the next step reaction (see Experimental Section). **P1** was first synthesized through the Sonogashira coupling reaction based on dibromo monomer **5** and double alkynyl monomer **3** with a molar ratio of 1.7:1. At beginning of the reaction, dibromo monomer and alkynyl monomer were added according to 1.5 eq. to 1 eq.. After 12 hours, another 0.2 eq. of dibromo monomer was added into the mixture to ensure **P1** was bromo-terminated polymer (Scheme 2) according to the reported end-capped control method [20]. The linear polymer (**P2**) was then prepared from (**P1**) and diallyl-POSS (molar ratio 1:1) through classic Heck coupling reaction. The conjugated length of **P2** was entirely depended on oligomeric alkynyl fluorene moiety from **P1**, and the molecular weight of **P2** was also controlled by column chromatography (see Experimental Section 2.2.8.).

Scheme 3. Synthesis of diallyl-POSS bridged linear polymer.



The molecular weight and distribution of polymers were investigated by GPC. Fig. 1 shows the retention time versus UV absorbance curves of **P1** and **P2**. The molecular weight of **P1** is $M_w = 8.79 \times 10^3$ Da and $M_n = 4.61 \times 10^3$ Da, while **P2** is $M_w = 3.93 \times 10^4$ Da and $M_n = 1.45 \times 10^4$ Da. The GPC data indicated the linear polycondensation reaction between **P1** and diallyl-POSS has happened.

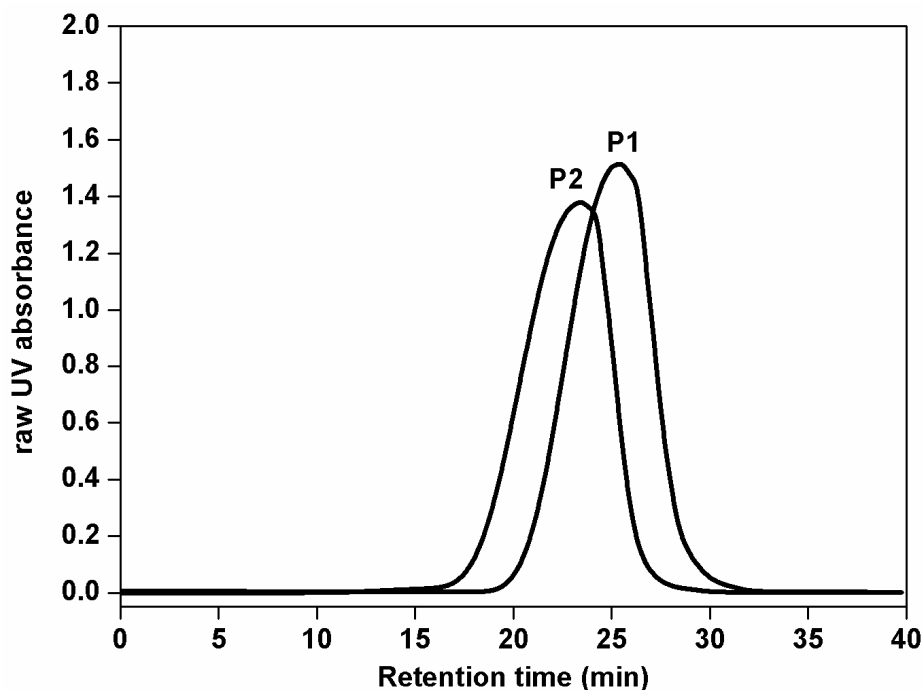


Fig. 1. GPC profiles of **P1** and **P2**.

The polycondensation reaction and the structures of **P1**, **P2** and diallyl-POSS were confirmed by the ^1H NMR (Fig. 2), solid ^{29}Si NMR, MALDI-TOF-MS and FT-IR spectra (see supplementary material). The proton peaks of **P1** at aromatic ring area are amplified and shown at $\delta \approx 8.09$ and $7.67\text{--}7.36$ ppm, respectively. While the broadening phenomenon of proton peak for **P2** could be observed at aromatic ring area, which are corresponded to the larger molecular weight of **P2**. The characteristic peak at 4.26 ppm belongs to the proton of methylene linking to carbazolyl for **P1** and **P2**. On the one hand, the characteristic peaks at $\delta \approx 5.76$ and $4.88\text{--}4.76$ ppm are corresponded to olefin proton of diallyl-POSS. For **P2**, the characteristic peak of olefin proton of diallyl-POSS moiety turns into a doublet and broad peak at 5.45 ppm with the integral area ratio of 1:1, which also confirms that **P2** has been synthesized and the Heck coupling reaction was successful. In the ^{29}Si NMR spectrum of **P2** (see supplementary material), **P2** displayed three broad characteristic signals at $\delta \approx -18.12$, -65.22 , and -79.10 ppm, respectively. The signal at -18.12 ppm is assignable to the silicon nucleus of $\text{Si}(\text{CH}_2\text{CH}=\text{CH})\text{CH}_3$ bond, and the signal at -65.22 ppm and -79.10 ppm belong to the other two kinds of the silicon nucleus of Si-O-Si cage. Furthermore, the FT-IR spectrum of **P2** shows an intense characteristic Si-O-Si stretching vibration at 1118 cm^{-1} for diallyl-POSS (see supplementary material). The characteristic signals at 3055 , 2923 , 2852 , 1681 ,

1663, and 1581 cm^{-1} respectively are corresponded to the oligomeric alkynyl fluorene moiety.

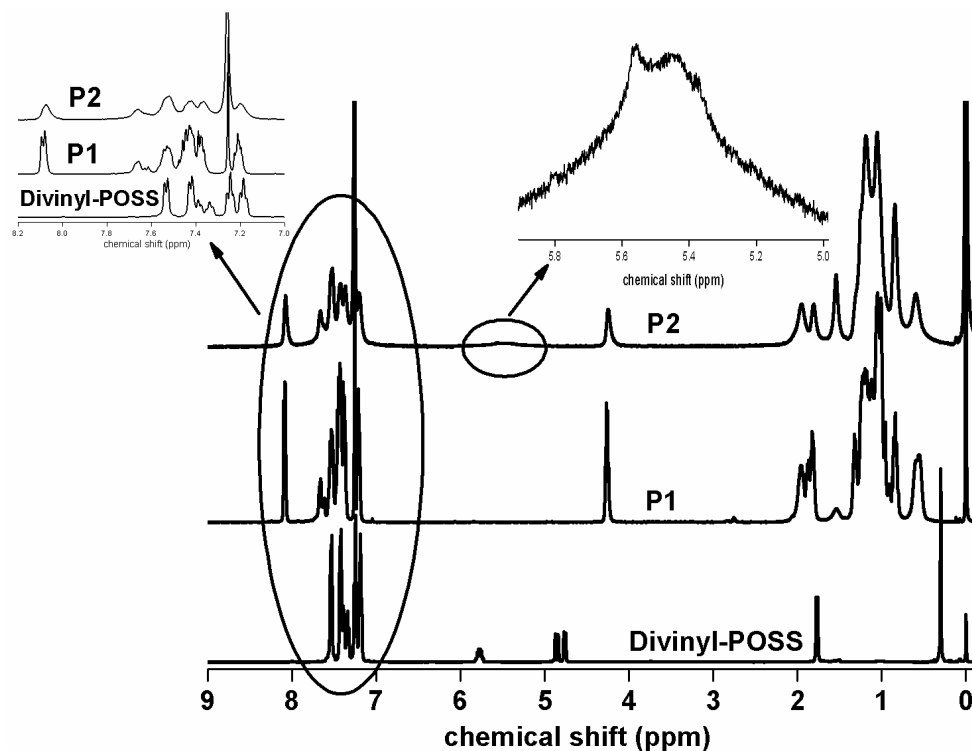


Fig. 2. The ^1H NMR spectra of **P1**, **P2** and diallyl-POSS.

3.2. Thermal Stability

The thermal stability of the polymers was measured via the thermogravimetric analysis (TGA) to study the influence of the introduction of diallyl-POSS. From TGA curves of **P1** and **P2** under nitrogen (Fig. 3), it was observed that the thermal decomposition temperature (T_d , 5% weight loss temperature) were 321 $^{\circ}\text{C}$ (**P1**) and 382 $^{\circ}\text{C}$ (**P2**), respectively. In other words, the T_d value of **P2** was 61 $^{\circ}\text{C}$ higher than that of **P1**. It indicates that the incorporation of diallyl-POSS can effectively enhance the thermal stability of the luminescent material due to the presence of inorganic Si–O cage shielding effect, which limits the heat transfer and protects the organic part of polymer from the heat effect of attack [21].

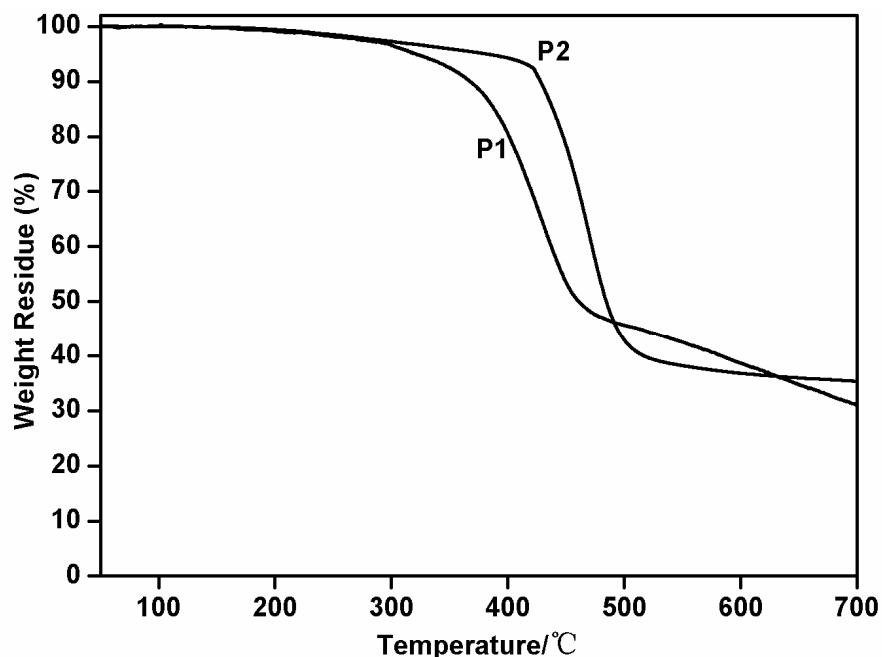


Fig. 3. TGA thermograms of **P1**, **P2**, at a ramp rate of 10 °C/min in nitrogen flow.

3.3. The morphologies of P1 and P2 films

HRTEM was used to analyze the microstructure of **P2** and **P1**. The diallyl-POSS connected to polyfluorene could be seen from the ultrathin sections of polymer embedded in epoxy resin. There are only a small quantity of 5–10 nm nanoparticles in **P2** sample [Fig. 4(a)], corresponding to diallyl-POSS aggregates. The same phenomenon can be seen in our previous work [22]. While a certain amount of smaller nanoparticles with the size of 2–3 nm are shown in the polymer matrix [Fig. 4(b) and 4(c)], which are uniformly nano-dispersed. It reveals that aggregation of the inorganic POSS could be reduced, in that diallyl-POSS is fixed on the main chain of polyfluorene via chemical bond and the bead-type POSS-based polymer has the symmetric structure. It could also benefit for attenuate the strong dipole-dipole and π - π stacking interactions between chromophores, which would acquire better properties for emissive conjugation polymers. This result has been further confirmed with AFM images (Fig. S1), in which the aggregation of diallyl-POSS multi-molecules are absent on the micron scale.

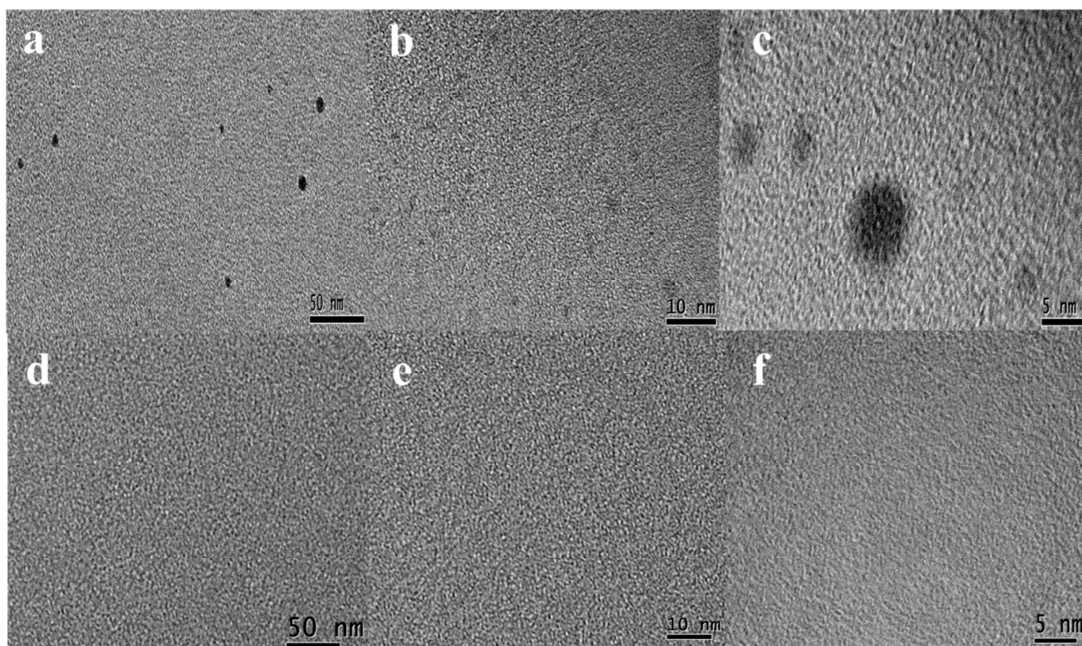


Fig. 4. HRTEM micrographs for **P2** (a, scale bar = 50 nm; b, scale bar = 10 nm; c, scale bar = 5 nm) and **P1** (d, scale bar = 50 nm; e, scale bar = 10 nm; f, scale bar = 5 nm).

3.4. Optical Properties

3.4.1. One-Photon Fluorescent Emission and Enhancement Fluorescent Quantum Yield (QY)

To study the impact of the incorporation of diallyl-POSS on the fluorescence emission of the fluorescent polymers, the one-photon fluorescence spectra of **P1** and **P2** both in solution and solid thin film state were acquired. The solid thin films of **P1** and **P2** were prepared by spin coating method on the quartz plate, and then, the PL spectra of **P1** and **P2** in thin solid film were measured (Fig. 5). The maximum emission peaks of **P1** and **P2** at 428 nm are similar in THF solutions, located at blue emission region. While in solid state, the aggregation effect leads to red shift of the main peaks to 538 nm (**P1**) and 475 nm (**P2**), respectively. Compared with **P1**, **P2** shows a larger blue-shift, which is attributed to the reduction of the molecular-stacking-led aggregations by the incorporation of large and rigid Si–O–Si cage [12b].

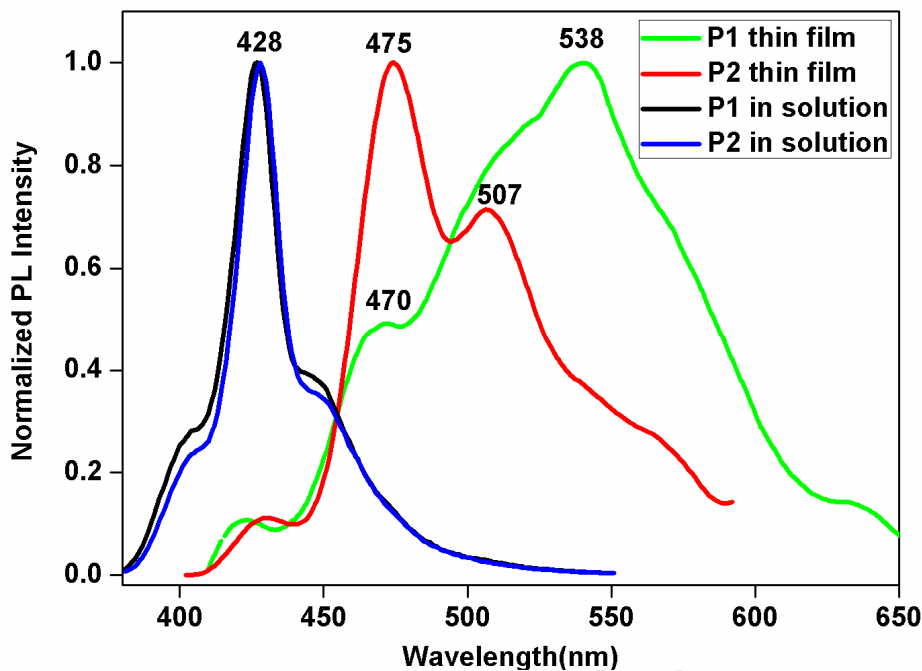


Fig. 5. The emission spectra of **P1** and **P2** in THF solutions and thin films.

Simultaneously, the QY of **P2** in dilute solution was calculated as 77.6% via reference method [23], which is higher than **P1** of 71.3% (Table S1). The QYs of **P1** and **P2** in solid state were also measured by a calibrated integrating sphere (ISF-513). The QY rises from **P1** of 3.1% to **P2** of 5.7%. The experimental results suggest that the oligomeric alkynyl fluorene moiety, when was nailed on the both ends of diallyl-POSS with highly symmetrical structure, can prevent the chromophoric groups close to each other, resulting the decreased emission quenching and the increased fluorescence quantum efficiency.

3.4.2. Two-photon Fluorescence Enhancement

To explore the two-photon fluorescence (TPF) enhancement effect of the incorporation of diallyl-POSS with symmetrical structure, the THF solutions of **P1** and **P2** with the same concentration (8.0×10^{-6} mol/L) of fluorescent groups (carbazole-fluorenyl and alkynyl-fluorenyl copolymer unit) were prepared, and the two-photon fluorescence spectra are shown in Fig. 6. Compared with **P1**, **P2** afforded the greater TPF enhancement. At the same time, taking emission peak at 428 nm as reference, the relative intensity of emission peak at 454 nm of **P2** was obviously weaker than that of **P1**. It reveals that, for **P2**, less excimers are formed in the solution

and the aggregation effect attenuates. The remarkable TPF enhancement could also be attributed to the abatement of aggregation effect between fluorescent groups when diallyl-POSS is coupled into polymer molecular chain.

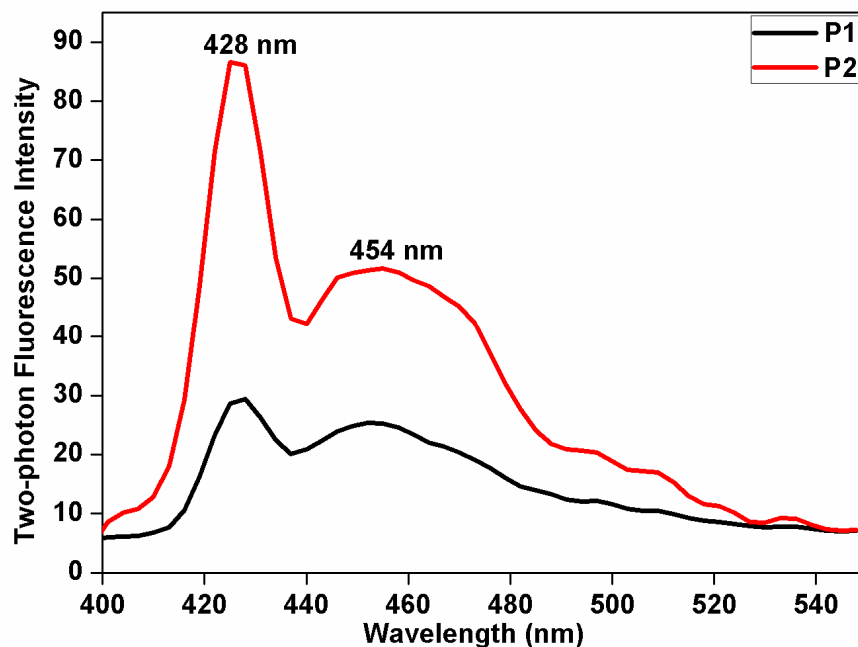


Fig. 6. The two-photon fluorescence spectra of **P1** and **P2** in THF solution with the same concentration of fluorescent groups (8.0×10^{-6} mol/L).

3.4.3. Photo-fading Experiment

Photo-stability is another crucial property for luminescent material, so photo-fading experiment of **P1** and **P2** (Fig. 7) is performed to probe the influence of incorporation of diallyl-POSS into the main chain of the light-emitting polymer. The THF dilute solutions of the polymers in 50 ml volumetric flasks were placed 25 cm from a 1000 W iodine-tungsten lamp. A cold trap (10 L solution of 50 g/L NaNO_2 and 20 cm in length) was set up between the sample and the lamp. The absorption spectra were recorded every 6 hours until 24 hours.

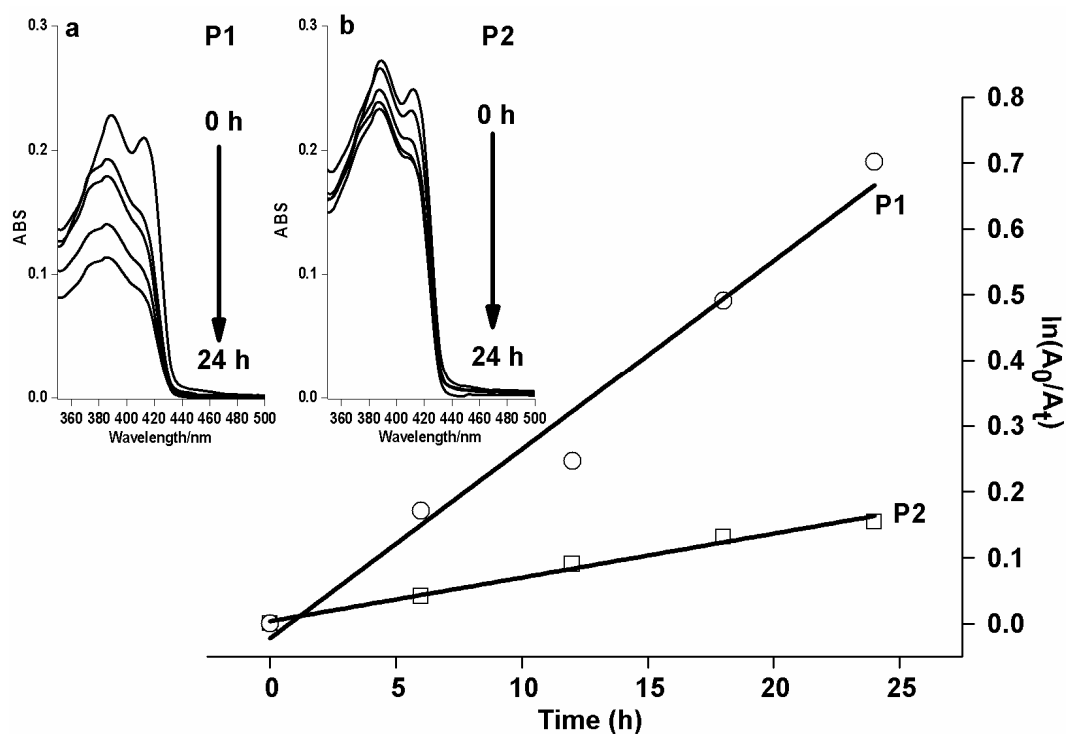


Fig. 7. The photo-degradation rate curves of **P1** and **P2**; Insert figures: The change of UV spectra under irradiation from a 1000 W iodine–tungsten lamp of a) **P1**, b) **P2** in THF at 25 °C.

From the inserted figure, the attenuation degree of the maximum absorption peak value of **P1** was obviously greater than that of **P2** over time. Under low concentration, photo-degradation equation can be simplified as $\ln(A_0/A_t) = kt$ [24], in which “ A_0 ” represents the initial absorption of λ_{\max} , “ A_t ” means the absorption of λ_{\max} during irradiation, and “ k ” is the photo-degradation reaction rate constant. Accordingly, “ k ” value could be acquired from the equation, and the fitting curves of “ $\ln(A_0/A_t)$ –Time” are given in Fig. 7. The slope of straight line after fitting is the photo-degradation reaction rate constant, and the “ k ” values of **P1** and **P2** are $k_{P1} = 4.8 \times 10^{-4}$ mol/min and $k_{P2} = 1.1 \times 10^{-4}$ mol/min, respectively (Table S3). Obviously, an enhanced photo-stability effect is obtained via the addition of diallyl-POSS into organic light-emitting material. Although the specific photo-stability enhancement mechanism is still unclear, it could be owing to the inorganic POSS nanoparticles, which is unfavorable towards photo-oxidation and stable against oxidation [25].

3.4.4. Decoupling Effect of the Hybrids under the State of Aggregation

Absorption spectra and fluorescence emission spectra of polymers in good/poor mixed solutions

were tested to explore the effect of aggregation for optical polymers according to the method reported in the literature [26]. In this regard, the polymers can form aggregations and excimers in THF/water solvents by adding different proportions of water. The absorption spectra and fluorescence emission spectra of **P1** and **P2** in THF and in mixed THF/water solvents were recorded.

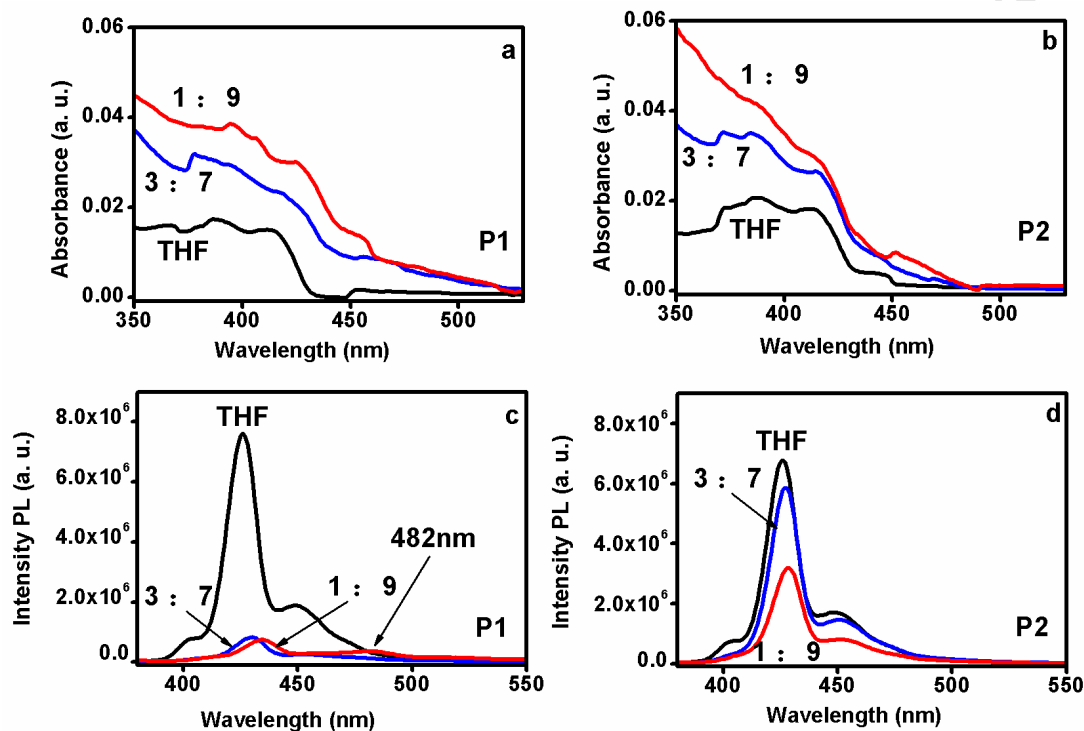


Fig. 8. Partial absorption spectra of a) **P1**, b) **P2** and photoluminescence spectra of c) **P1**, d) **P2** in THF, THF–water (3:7, v/v), and THF–water (1:9, v/v).

As shown in Figure 8a and 8b, both **P1** and **P2** molecular chains can be well-dispersed in the dilute THF solution due to the weak intermolecular interaction. Nevertheless, the absorbances at λ_{\max} of **P1** and **P2** are obviously enhanced and undergo red shift with the increase of water content (3:7 v/v and 1:9 v/v THF–water), which indicates that the two polymers have formed J-type aggregations [27].

On the other hand, the conspicuous emission quenching of **P1** by adding different proportions of water in THF were observed. The excimer peak at 482 nm in the **P1** emission spectra appeared clearly in a 1:9 (v/v) THF–water mixed solvent [Figure 8(c)]. The fluorescence emission intensity of **P2** in 3:7 (v/v) and 1:9 (v/v) THF–water is much greater than that of **P1**, and the emission spectra of **P2** still has no excimer peak in a 1:9 (v/v) THF–water mixed solvent [Fig. 8(d)]. These

results indicate that the optical property of **P2** is stable in THF/water solvents owing to the incorporation of diallyl-POSS, while that of **P1** is not.

Simultaneously, the QY values of **P2** are 23.8% and 12.3% in 3:7 (v/v) and 1:9 (v/v) THF–water mixed solvent respectively, which are much higher than those of **P1** (10.6% and 4.9%, Table S1). It suggests that the strong dipole–dipole and π – π stacking interactions between organic optical chromophoric groups can lead to forming J-type aggregations, which would affect luminescent properties and application of light emitting polymers. Therefore, the incorporation of “huge” and “rigid” diallyl-POSS into optical materials via chemical bonds to form bead-type condensation polymer can effectively improve the optical performances under the state of aggregation.

3.5. Fluorescent Composite Film

The fluorescence composite films of **P1** and **P2** were prepared, and the purpose of which was to lay the foundation for the application of difunctional-POSS based polymer in developing new photoelectric material. In this paper, fluorescence composite films were fabricated using the 3-isocyanatomethyl-3,5,5-trimethylcyclohexyl isocyanate (IPDI) and poly-caprolactone diol (PCL M_w 1000) as matrix, and doped with different proportions of light-emitting polymer molecules (Fig. 9). The influence of doped mass fraction of **P1** and **P2** on PL spectra of the fluorescent composite films was investigated to elucidate the effect of incorporation of diallyl-POSS into luminescent material (Fig. 10). Meanwhile, the QYs of fluorescent composite film with different doped mass fractions of **P1** and **P2** were measured, and photoluminescence spectra were also obtained (Table S4). There was no obvious change for PL spectra when the mass fractions of **P1** and **P2** were 1×10^{-6} and 5×10^{-6} . The maximum emission peaks of **P1** and **P2** were both located at 427 nm, which are similar to **P1** and **P2** in dilute solution. This phenomenon shows that the aggregation of fluorescent groups does not appear when the fluorescence composite films doped with low mass fraction of **P1** and **P2**.

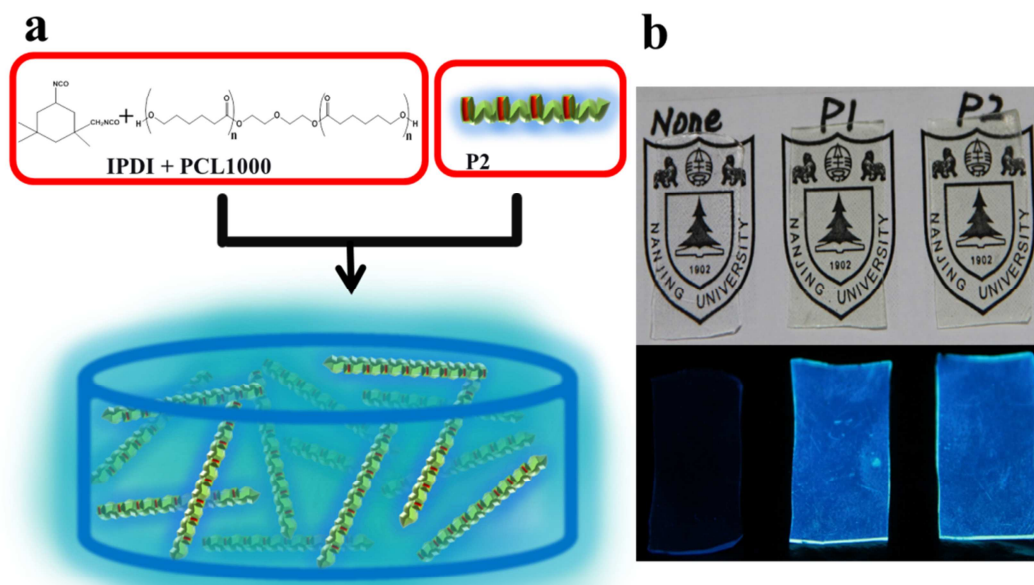


Fig. 9. a) Schematic illustration of preparation of fluorescent composite films (taking **P2** for example); b) The fluorescent composite film doped with 5×10^{-5} mass fraction of **P1** and 1×10^{-4} mass fraction of **P2** under sunlight and 365 nm UV-light.

Compared with fluorescent composite films of **P2**, the emission spectra of **P1** fluorescent composite films showed larger red shift and more excimer peaks in longer wavelength with the increase of the mass fraction of **P1**. It reveals that a more serious aggregation effect of fluorescent groups has occurred in the fluorescent composite films of **P1**. Furthermore, the intensity of excimer emission peak at 535 nm increased dramatically when composite film doped with higher mass fraction of **P1** (1×10^{-3} and 5×10^{-3}), while the composite film of **P2** merely showed a weak shoulder peak at 535 nm under the same conditions. This is a powerful evidence to demonstrate that the strong dipole–dipole and π – π stacking interactions between organic optical chromophoric groups are suppressed owing to the introduction of diallyl-POSS.

Meanwhile, the maximum QY of **P1** fluorescent composite film was 18.8% as doped with 5×10^{-5} mass fractions of **P1**, while that of **P2** was 20.5% as doped with 1×10^{-4} mass fractions of **P2**. Namely, the maximum QY of the fluorescent composite film of **P2** appears at higher doped mass fraction (1×10^{-4}) than that of **P1** fluorescent composite film (5×10^{-5}), which insinuates that the incorporation of “huge” and “rigid” diallyl-POSS could prevent excessive aggregation in solid

state. The diallyl-POSS bridged polyfluorene hybrid material with symmetrical structure has higher QY.

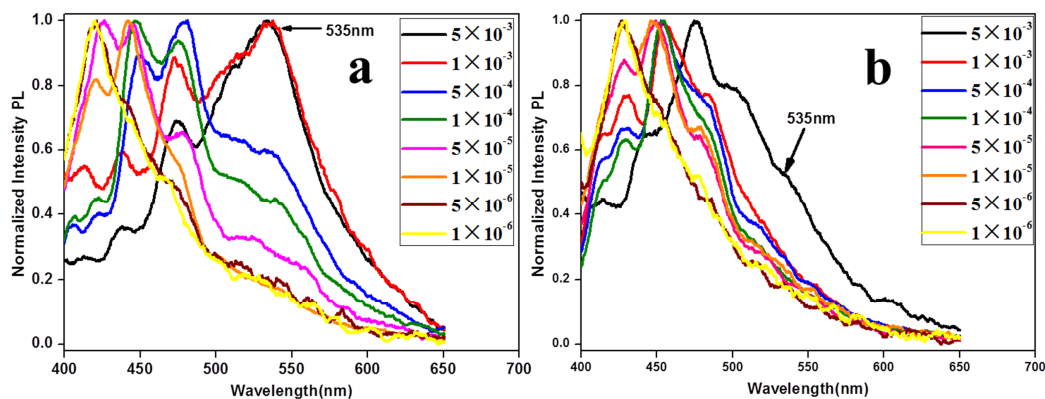


Fig. 10. The PL spectra of fluorescent composite films with different mass fractions of a) P1 and b) P2.

No microphase separation was observed when QYs of fluorescent composite films of **P1** and **P2** reached the maximum (Fig. 9 and Fig. S2), and the fluorescent composite films of **P1** and **P2** showed excellent TPF property and could be applied in real-time 3D high-resolution TPF imaging (Fig. S3).

4. Conclusion

In summary, a bead type and diallyl-POSS based polyfluorene (**T₈D₂** type) with high symmetrical structure (**P2**) was synthesized via Heck coupling reaction. The molecular weight of **P1** and **P2** was well controlled to provide the polymers with good solubility and process ability. The HRTEM micrographs showed that diallyl-POSS was uniformly nano-dispersed in the polymer matrix. And the thermal decomposition temperature (T_d , 5% loss) increased from 321 °C for **P1** to 382 °C for **P2**.

Simultaneously, the well-controlled conjugated length gave **P1** and **P2** with high QYs, and cooperating “rigid”, “symmetrical” and “huge” diallyl-POSS could further enhance quantum efficiency in solution and solid state. The rate constants of photo-degradation reaction under a 1000 W iodine–tungsten lamp were $k_{p1} = 4.8 \times 10^{-4}$ mol/min and $k_{p2} = 1.1 \times 10^{-4}$ mol/min, respectively, which confirmed the significantly enhanced photo-stability by adding unfavorable photo-oxidation diallyl-POSS to emissive conjugated polymer. Moreover, a better TPF property was found for **P2**, which could also be attributed to the incorporation of diallyl-POSS, and the

strong dipole–dipole and π – π stacking interactions between organic optical chromophoric groups could be inhibited. Finally, fluorescent composite films were prepared, and the maximum QY of **P2** reached to 20.5%. These results suggest that bi-functional POSS based polymer may be considered a class of compounds/materials with anticipated novel properties of value in developing new components for electronic and photonic applications.

Acknowledgements

This work was supported by the National Natural Science Foundation of China (Grant No.21104032), the Natural Science Foundation of Jiangsu Province (No. BK2011413), the Fundamental Research Funds for the Central Universities (No. 1104020505) and the Postgraduate Research and Innovation Project of Jiangsu Province (2014, No. KYLX_0030). The authors would like to thank the Program for Changjiang Scholars and Innovative Research Team in University for financially supporting this research.

Appendix. Supplementary material

Supplementary data related to this article can be found online.

References:

- [1] (a) Günes S, Neugebauer H, Sariciftci NS. *Chem Rev* 2007; 107: 1324–38;
(b) Zhong H, Durrant JR, Heeney M, et al. *J Am Chem Soc* 2013; 135: 2040–3;
(c) Earmme T, Subramaniyan S, Jenekhe SA, et al. *J Am Chem Soc* 2013; 135: 14960–3;
(d) Biniek L, Anthopoulos TD, McCulloch I, et al. *Macromolecules* 2013; 46: 727–35;
(e) Liang L, Mei CY, Li WS, et al. *Polymer* 2013; 54: 2278–84.
- [2] (a) Liu J, Lam JWY, Tang BZ. *Chem Rev* 2009; 109: 5799–867;
(b) Chen X, Liao L, Chen A, et al. *J Am Chem Soc* 2003; 125: 636–7;
(c) Davis AR, Maegerlein JA, Carter KR. *J Am Chem Soc* 2011; 133: 20546–51;
(d) Gu C, Dong W, Yao L, Ma Y, et al. *Adv Mater* 2012; 24: 2413–7.
(e) Gu C, Fei T, Ma Y, et al. *Adv Mater* 2010, 22: 2702–5.
- [3] (a) Wu C, Chiu DT. *Angew Chem Int Ed* 2013; 52: 3086–109;
(b) Ye F, Wu C, Chiu DT, et al. *J Am Chem Soc* 2011; 133: 8146–9;

- (c) Musyanovych A, Landfester K. *Macromol Biosci* 2014, 14: 458–77.
- [4] (a) Wu T, Barker M, Branda NR, et al. *Angew Chem Int Ed* 2013; 52: 11106–9;
(b) Navarro JRG, Andrauda C, Parolaa S, et al. *Biomaterials* 2013; 34: 8344–51;
(c) Oha I, Kimb K, Huh KM, et al. *Biomaterials* 2013; 34: 6454–63.
- [5] (a) Wang J, Mei J, Tang BZ, et al. *Macromolecules* 2012, 45: 7692–703;
(b) Hu R, Lam JW, Tang BZ, et al. *Polym Chem* 2013, 4: 95–105;
(c) Gao M, Lam JW, Tang BZ, et al. *Polym. Chem* 2013, 4: 1372–80.
- [6] (a) Fischer CS, Baier MC, Mecking S. *J Am Chem Soc* 2013; 135: 1148–54;
(b) Senthilkumar T, Asha SK. *Macromolecules* 2013; 46: 2159–71;
(c) Yang PJ, Chu HC, Lin HC, et al. *Polymer* 2012; 53: 939–46;
(d) Ibnaouf KH, Masilamani V, AlSalhi MS, et al. *Polymer* 2013; 54: 2401–5;
(e) Prasad S, Masilamani V, AlSalhi MS, et al. *Polymer* 2014; 55: 727–32;
(f) Shi H, Liu B, Huang W, et al. *Adv Funct Mater* 2013; 23: 3268–76.
- [7] (a) Zhu C, Liu L, Wang S, et al. *Chem Rev*, 2012; 112: 4687–735;
(b) He F, Ren X, Xu Q, et al. *Macromolecules* 2011; 44: 5373–80.
- [8] (a) Xu B, Tong H, Wang L, et al. *Polymer* 2012; 53: 490–4;
(b) Knaapila M, Monkman AP. *Adv Mater* 2013; 25: 1090–108;
(c) Wang ZJ, Landfester K, Zhang KAI, *Chem Commun* 2014; 50: 8177–80.
- [9] (a) Intemann JJ, Hellerich ES, Jeffries-EL M, et al. *Macromolecules* 2012; 45: 6888–97;
(b) Chuang CN, Leung M, Hsieh KH, et al. *Polymer*, 2012; 53: 2001–7;
(c) Song HJ, Lee JY, Moon DK, et al. *Polymer* 2013; 54: 1072–9;
(d) Xie LH, Hou XY, Huang W, et al. *J Am Chem Soc* 2008; 130: 2120–1;
(e) Lin WP, Liu SJ, Huang W, et al. *Adv Mater* 2014; 26: 570–606.
- [10] (a) Thomas SW, Joly GD, Swager TM. *Chem Rev* 2007; 107: 1339–86;
(b) Lin NB, Liu XY, Xu HY, et al. *Adv Funct Mater* 2012; 22: 361–8;
(c) Woo HY, Liu B, Bazan GC, et al. *J Am Chem Soc* 2005; 127: 14721–9;
(d) Yu WL, Huang W, Heeger AJ, et al. *Adv Mater* 2000; 12: 828–31;
(e) Zeng G, Chua SJ, Huang W, et al. *Macromolecules* 2002; 35: 6907–14.
- [11] (a) Liu XM, Xu J, He CB, et al. *Macromolecules* 2006; 39: 1397–402;
(b) Wu CW, Lin HC. *Macromolecules* 2006; 39: 7232–40;

- (c) Wang HY, Huang W, Wei W, et al. *J Phys Chem C* 2011; 115: 6961–7;
- (d) Huang F, Zhang Y, Jen AKY, et al. *Adv Funct Mater* 2007; 17: 3808–15;
- (e) Liu C, Qin J, Cao Y, et al. *Chem Mater* 2013; 25: 3320–7.
- [12] (a) Cordes DB, Lickiss PD, Rataboul F. *Chem Rev* 2010; 110: 2081–173.
- (b) Xiao S, Cao Y, Heeger AJ, et al. *Adv Funct Mater* 2003; 13: 25–9.
- [13] (a) Zhu C, Lv F, Wang S, et al. *Chem Rev* 2012; 112: 4687–735;
- (b) Yang X, Froehlich JD, Jabbour GE, et al. *Adv Funct Mater* 2009; 19: 2623–9;
- (c) Araki H, Naka K. *Macromolecules* 2011; 44: 6039–45;
- (d) Su XY, Xu HY, Liu XY, et al. *Macromolecules* 2010; 43: 2840–5.
- [14] R. Corriu, P. Jutzi, editors. *Tailor-Made Silicon-Oxygen Compounds: from Molecules to Materials*, P 196: Springer-Verlag Berlin and Heidelberg GmbH & Co. K; 1996.
- [15] (a) Lin WJ, Chen WC, Jen AKY, et al. *Macromolecules* 2004; 37: 2335–41;
- (b) Cho HJ, Hwang DH, Shim HK, et al. *Chem Mater* 2006; 18: 3780–7.
- [16] (a) Lee J, Cho HJ, Shim HK, et al. *Macromolecules* 2004; 37: 8523–29;
- (b) Leea J, Hwangb DH, Shim HK, et al. *Synth Met* 2006; 156: 590–6;
- (c) Chou CH, Hsu SL, Wei KH, et al. *Macromolecules* 2005; 38: 745–51;
- (d) Pu KY, Fan QL, Huang W, et al. *Polymer* 2006; 47: 1970–8.
- [17] (a) Sellinger A, Tamaki R, Laine RM, et al. *Chem Commun* 2005; 29: 3700–2;
- (b) Pu KY, Xie J, Liu B, et al. *J Phys Chem C* 2011; 115: 13069–75;
- (c) Pu KY, Li K, Liu B. *Adv Mater* 2010; 22: 643–46.
- [18] (a) Laine RM, Sulaiman S, Goodson T, et al. *Chem Mater* 2008; 20: 5563–73;
- (b) Laine RM, Rand SC, Li Y, et al. *J Am Chem Soc* 2010; 132: 3708–22;
- (c) Laine RM, Furgal JC, Goodson T, et al. *J Am Chem Soc* 2013; 135: 12259–69;
- (d) Laine RM, Furgal JC, Goodson T, et al. *Macromolecules* 2013; 46: 7591–604.
- [19] Haj FG, Verveer PJ, Bastiaens PIH, et al. *Science* 2002; 295: 1708–11.
- [20] (a) Basak S, Narayana YSLV, Chandrasekar R, et al. *Macromolecules* 2013; 46: 362–9;
- (b) Kuo CH, Cheng WK, Hsieh KH, et al. *J Polym Sci Pol Chem* 2007; 45: 4504–13.
- [21] (a) Asuncion MZ, Laine RM. *Macromolecules* 2007; 40: 555–62;
- (b) Markovic E, Hussain M, Simon GP. *Macromolecules* 2007; 40: 2694–701.
- [22] Zhang QH, Yu XH, Jia XD, et al. *Macromolecules* 2011; 44: 550–7.

- [23] Olmsted J. *J Phys Chem* 1979; 83: 2581–4.
- [24] (a) Chen P, Qian Z, Zheng D, et al. *Dyes Pigments* 1999; 41: 227–31;
(b) Chen X, Wang L, Zhang R, et al. *J Photoch Photobio A* 2006; 181: 79–85.
- [25] (a) Kang JM, Hwang DH, Shim HK, et al. *Macromolecules* 2006; 39: 4999–5008;
(b) Brown AS. *Aerosp Am* 1999; 37: 30–3.
- [26] (a) Chen HJ, Farahat MS, Whitten DG, et al. *J Am Chem Soc* 1996; 118: 2584–94;
(b) Yan ZQ, Xu HY, Liu XY, et al. *Adv Funct Mater* 2012; 22: 345–52.
- [27] (a) Eisfeld A, Briggs JS. *Chem Phys* 2006; 324: 376–84;
(b) Law Y. *Chem Rev* 1993; 93: 449–86.

Supplementary data for

New Bead Type and High Symmetrical Diallyl-POSS Based Emissive Conjugated Polyfluorene

Jin Huang,^{a,b} Weina Wang,^{a,b} Jiangjing Gu,^{a,b} Weizhi Li,^{a,b} Qihong Zhang,^{a,b} Yin Ding,^c Kai Xi,^b
Youxuan Zheng,^a Xudong Jia^{*a,b}

^aState Key Laboratory of Coordination Chemistry, Nanjing National Laboratory of Microstructures, Nanjing University, Nanjing 210093, PR China

^bDepartment of Polymer Science & Engineering, Nanjing University, Nanjing 210093, PR China

^cState Key Laboratory of Analytical Chemistry for Life Science, Nanjing University, Nanjing 210093, PR China

*correspondence to: Xudong Jia (jiaxd@nju.edu.cn)

1. Morphology observation

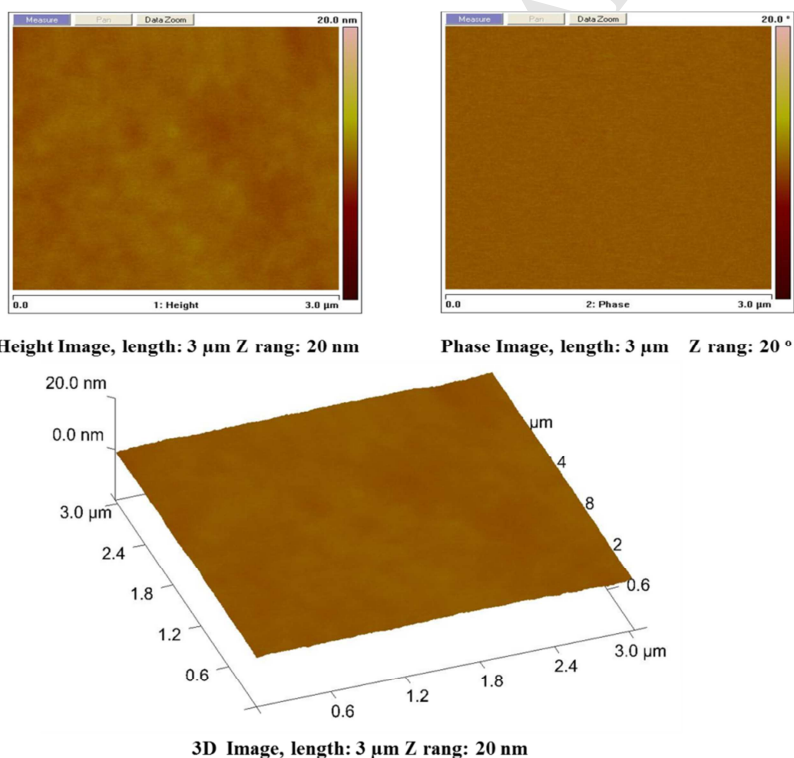


Fig. S1. AFM height images, phase images and 3D image of P2.

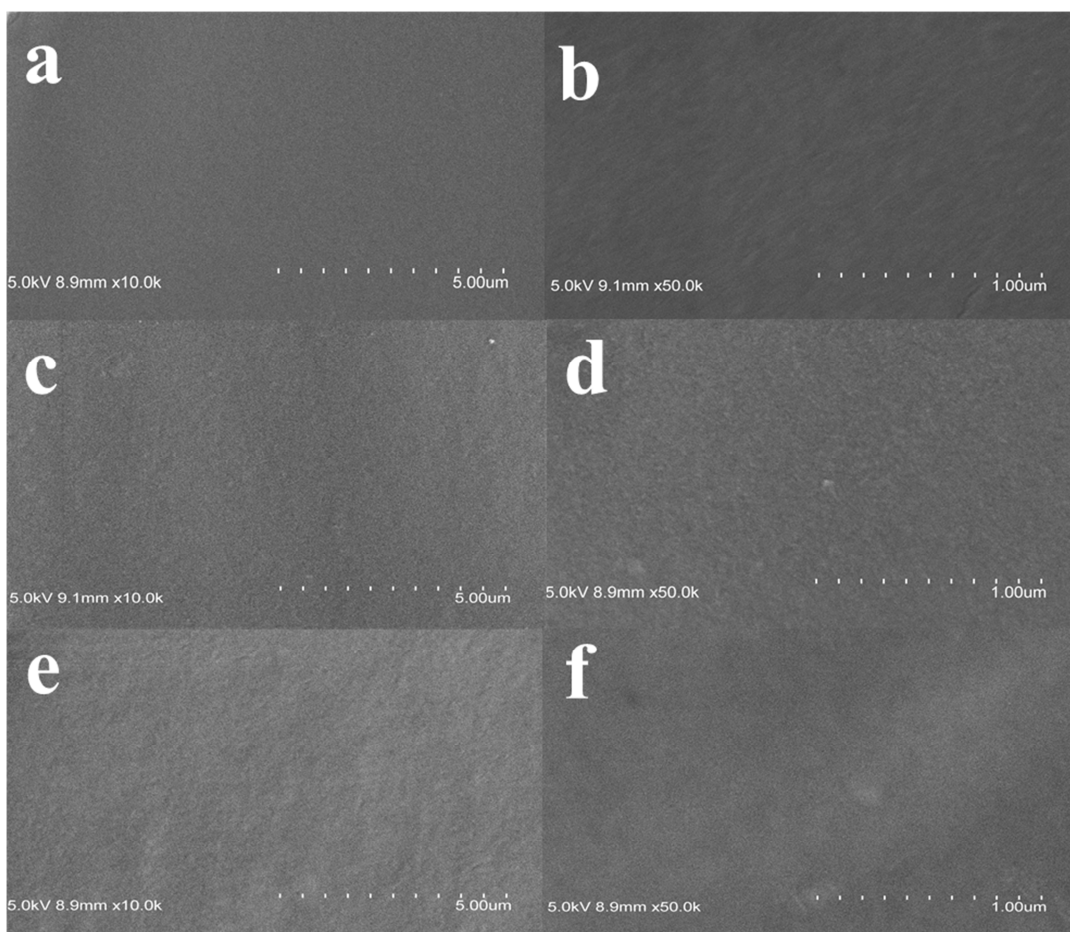


Fig. S2. The scanning electron microscopy (SEM) image of blank sample (IPDI+PCL1000) a) and b), the mass fraction of 5×10^{-5} P1 c) and d), and the mass fraction of 10^{-4} P2 e) and f) fluorescent composite film.

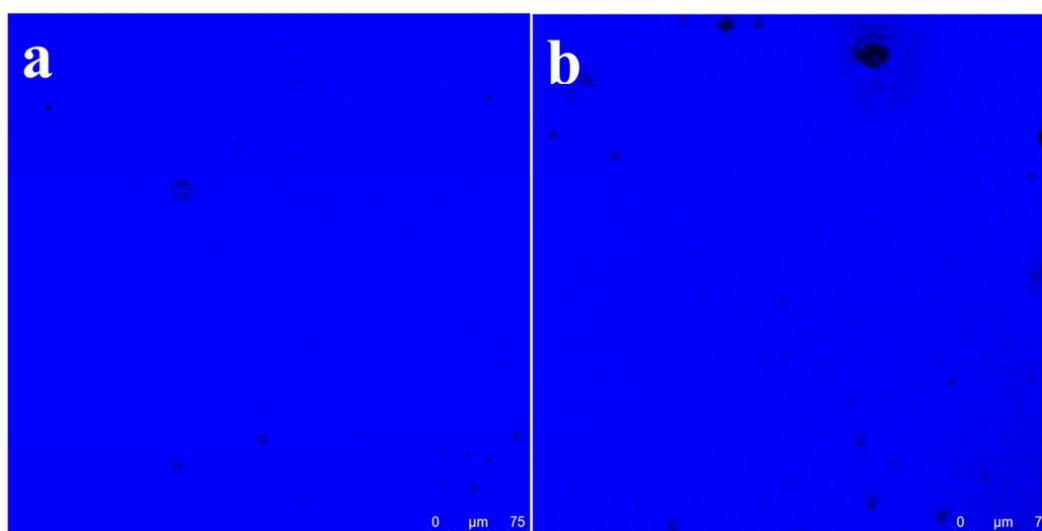


Fig. S3. Two-photon fluorescence imaging of P1 (the mass fraction of 5×10^{-5}) and P2 (the mass fraction of 10^{-4}) fluorescent composite film.

2. Fluorescence quantum yield (Φ) measurements

Fluorescence quantum yield (Φ) of P1 and P2 was obtained by the following steps. Quinine sulfate was dissolved in 0.1 M sulphuric acid (literature quantum yield 0.54 at 360 nm) as reference.¹ Then UV-vis absorption and PL emission spectra (with 360nm excitation) of P1 and P2 with different solvent and reference were measured respectively. The accurate Φ value was calculated according to the given equation:

$$\Phi_{sam} = \Phi_{ref} \frac{I_{sam} A_{ref} n_{sam}^2}{I_{ref} A_{sam} n_{ref}^2}$$

“Sam” and “ref” refer to sample and reference respectively. “ Φ ” means quantum yield. “I” is the integrated emission intensity, and could be calculated from the emission spectra at 360nm excitation. “A” represents UV-vis absorbance at 360 nm and was control under 0.05 in the 10 mm quartz to avoid re-absorption effect. “n” is the refractive index.

Table S1. Fluorescence quantum yield (Φ) calculation of the fluorescent for deaggregation effect of the Hybrids.

Sample	Intergrated emission intensity (I)	UV Absorbance (A)	Refractive index of solvent (n)	Fluorescence quantum efficiency (Φ)
Quinine sulfate	120647590	0.0112	1.33	54.0
P1 THF	197462540	0.0156	1.41	71.3
P1 water content 70 %	64703405	0.0321	1.36	10.6
P1 water content 90 %	39925305	0.0418	1.34	4.9
P2 THF	179073260	0.0130	1.41	77.6
P2 water content 70 %	151783080	0.0334	1.36	23.8
P2 water content 90 %	10910340	0.0450	1.34	12.3

3. Photofading experiment

Table S2. The $\ln(A_0/A_t)$ -Time values of P1 and P2.

P 1	$\ln(A_0/A_t)$	P 2	$\ln(A_0/A_t)$
Time (h)		Time (h)	
0	0	0	0
6	0.17073	6	0.04127
12	0.24632	12	0.08992
18	0.49101	18	0.13139
24	0.70151	24	0.15427

4. The QYs of fluorescent composite films

Table S3. The QYs of fluorescent composite films.

P1 Mass fraction	QY (%)	P2 Mass fraction	QY (%)
5×10^{-3}	15.1	5×10^{-3}	15.3
1×10^{-3}	16.3	1×10^{-3}	15.8
5×10^{-4}	17.1	5×10^{-4}	19.7
1×10^{-4}	17.8	1×10^{-4}	20.5
5×10^{-5}	18.8	5×10^{-5}	17.9
1×10^{-5}	10.2	1×10^{-5}	15.6
5×10^{-6}	7.6	5×10^{-6}	10.9
1×10^{-6}	7.2	1×10^{-6}	10.3

5. Synthesis and Characterization

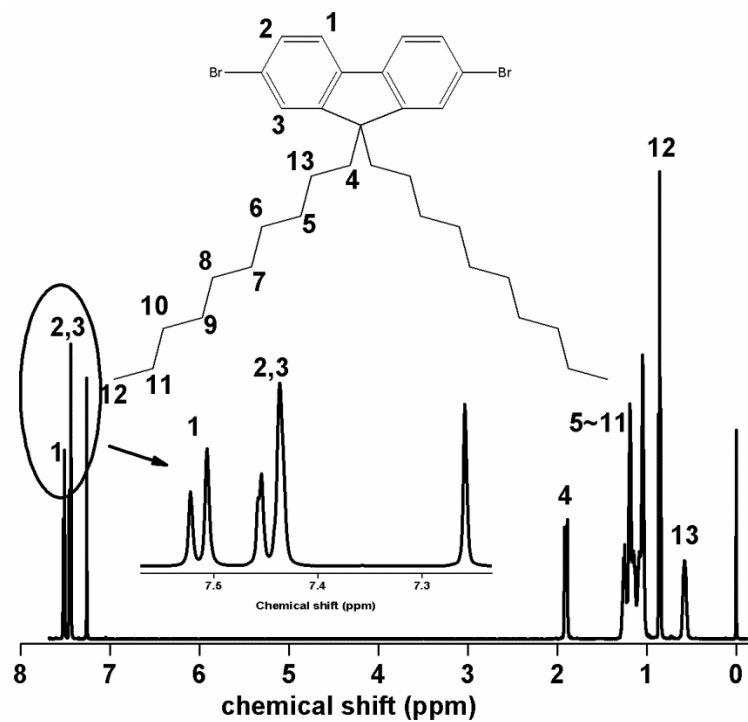


Fig. S4. The ^1H NMR spectra of 2,7-dibromo-9,9-didecyl-9H-fluorene. (500 MHz, CDCl_3)

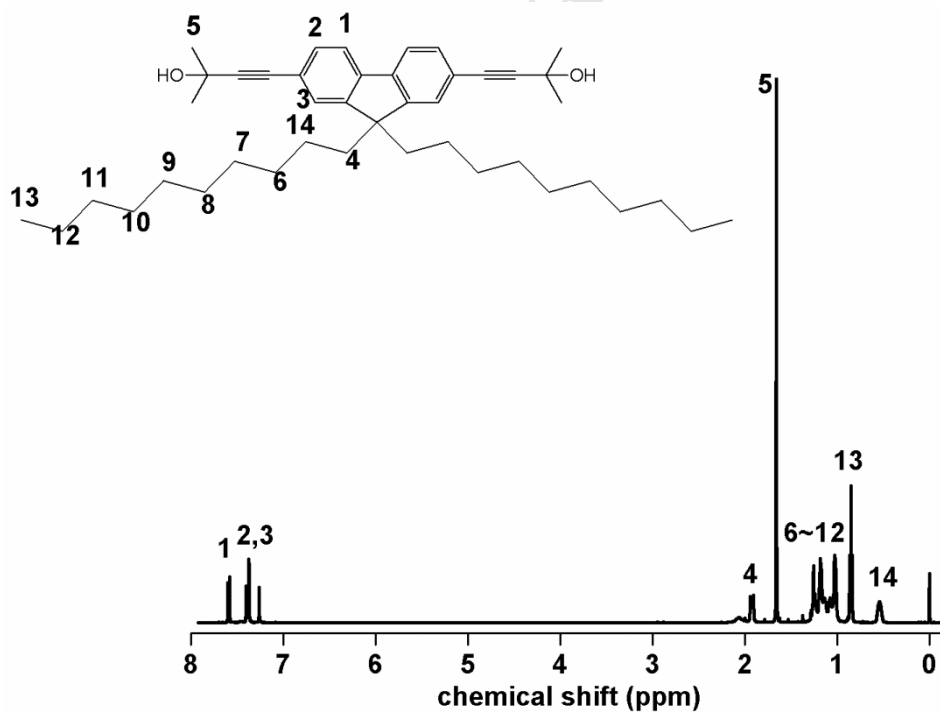


Fig. S5. The ^1H NMR spectra of 4,4'-(9,9-didecyl-9H-fluorene-2,7-diyl)bis(2-methylbut-3-yn-2-ol). (500 MHz, CDCl_3)

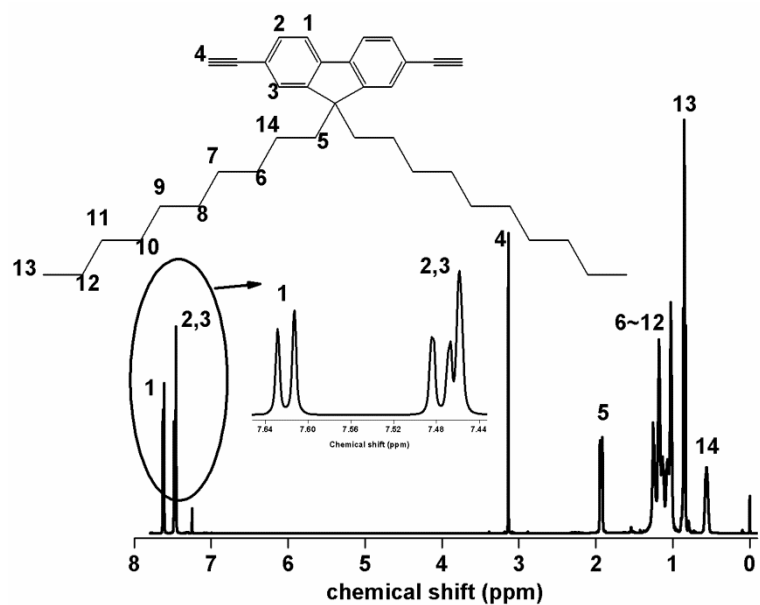


Fig. S6. The ^1H NMR spectra of 9,9-didecyl-2,7-diethynylfluorene. (500 MHz, CDCl_3)

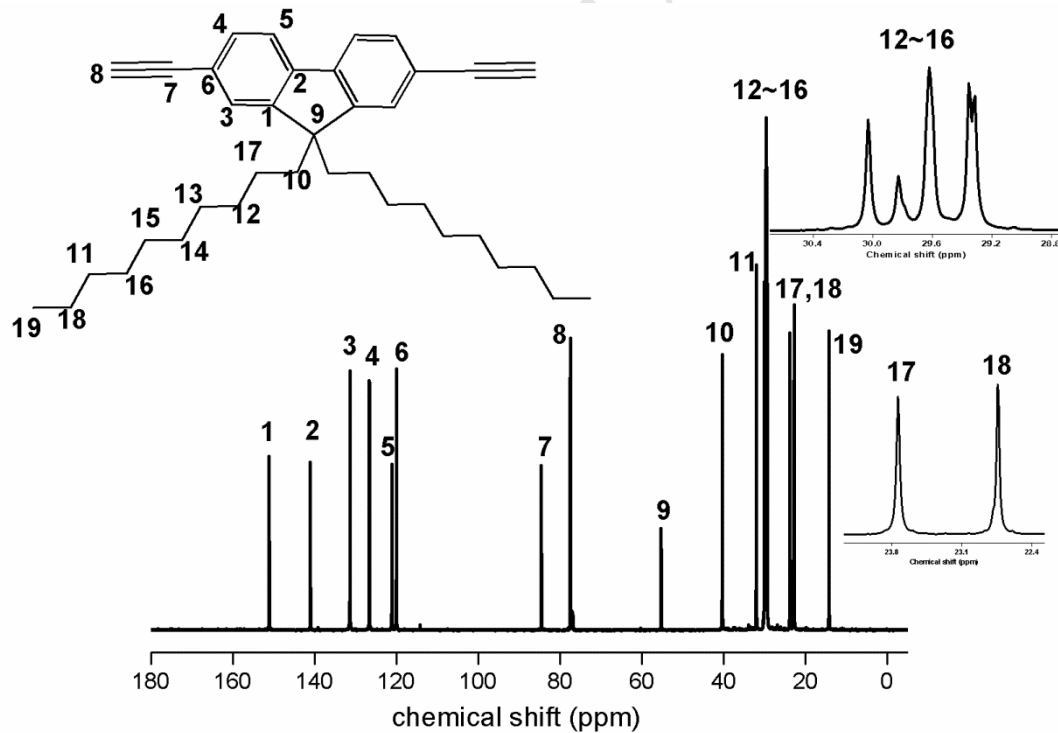


Fig. S7. The ^{13}C NMR spectra of 9,9-didecyl-2,7-diethynylfluorene. (500 MHz, CDCl_3)

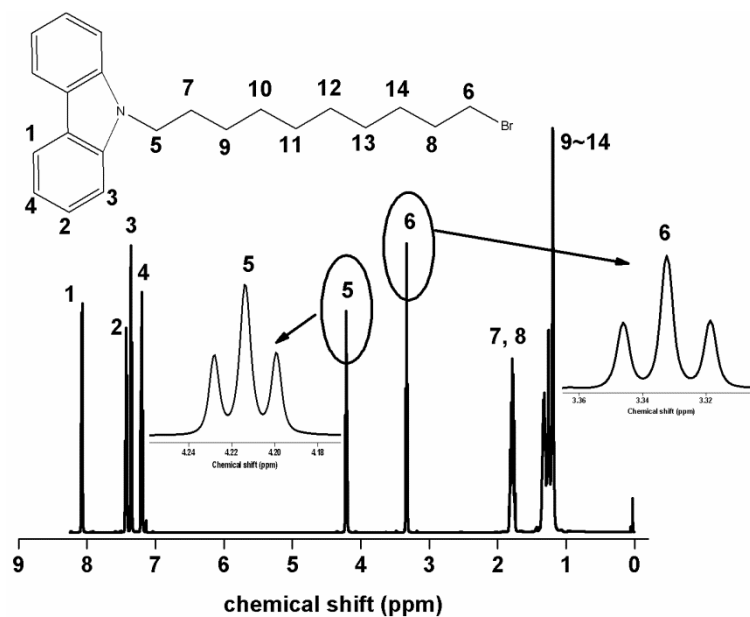


Fig. S8. The ^1H NMR spectra of 9-(10-bromodecyl)-9H-carbazole. (500 MHz, CDCl_3)

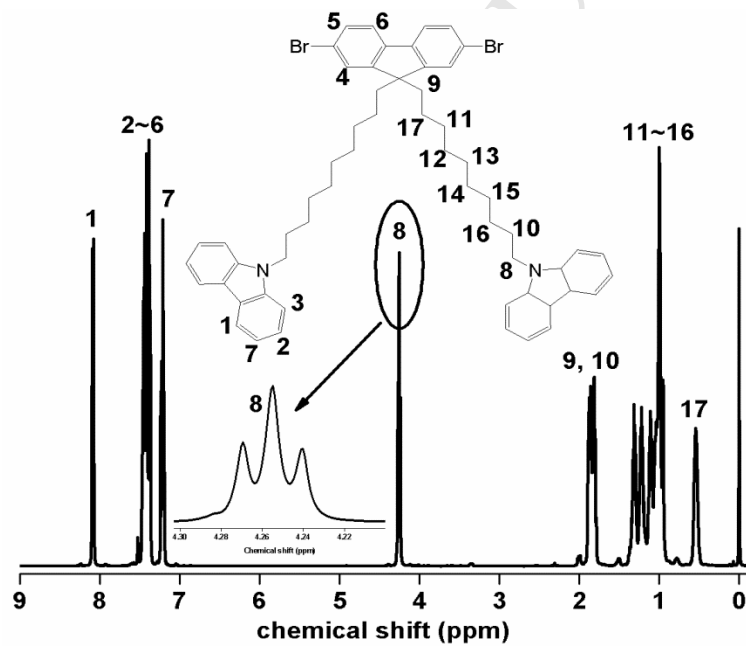


Fig. S9. The ^1H NMR spectra of 9,9'-(2,7-dibromo-9H-fluorene-9,9-diyl)bis(decane-10,1-diyl)bis(9H-carbazole). (500 MHz, CDCl_3)

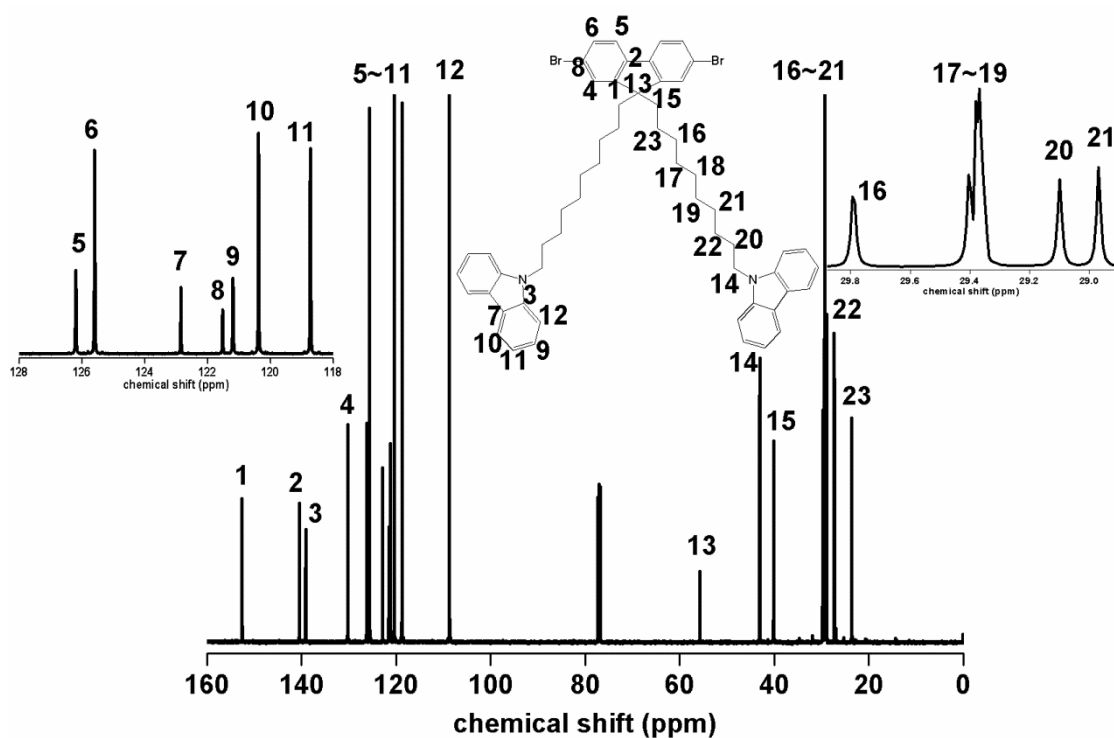


Fig. S10. The ^{13}C NMR spectra of 9,9'-(2,7-dibromo-9H-fluorene-9,9-diyl)bis(decane-10,1-diyl)bis(9H-carbazole). (500 MHz, CDCl_3)

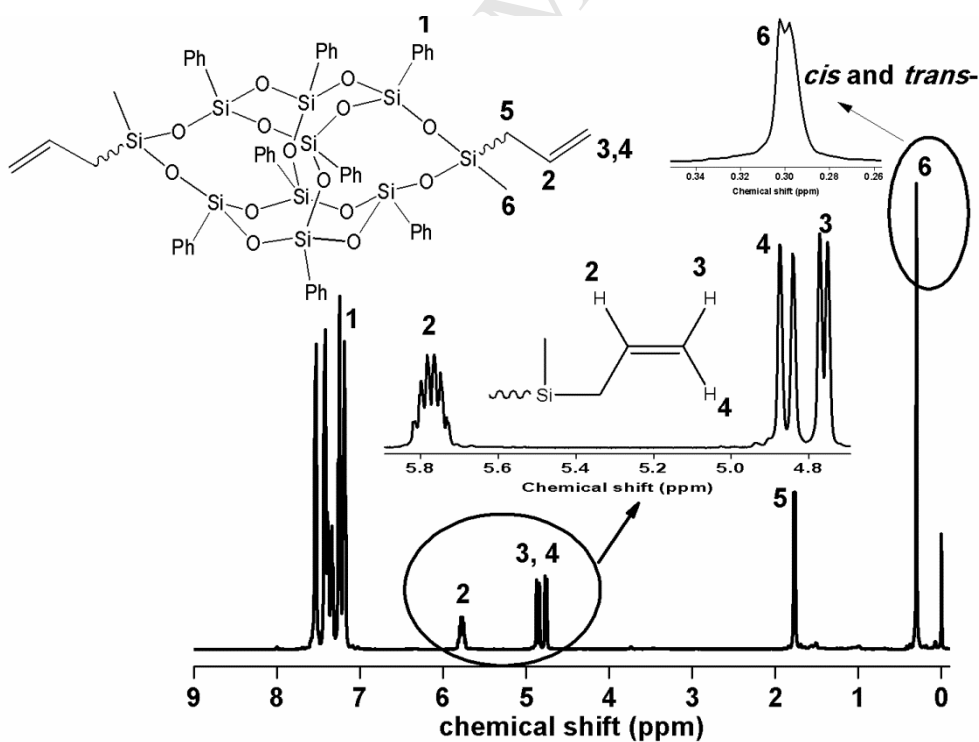


Fig. S11. The ^1H NMR spectra of 3,13-di(3-propenyl)-3,13-dimethyl-1,5,7,9,11,15,17,19-octaphenylhexacyclo[15.3.1(1,13).1(3,11).1(5,17).1(9,15)]decasiloxane. (500 MHz, CDCl_3)

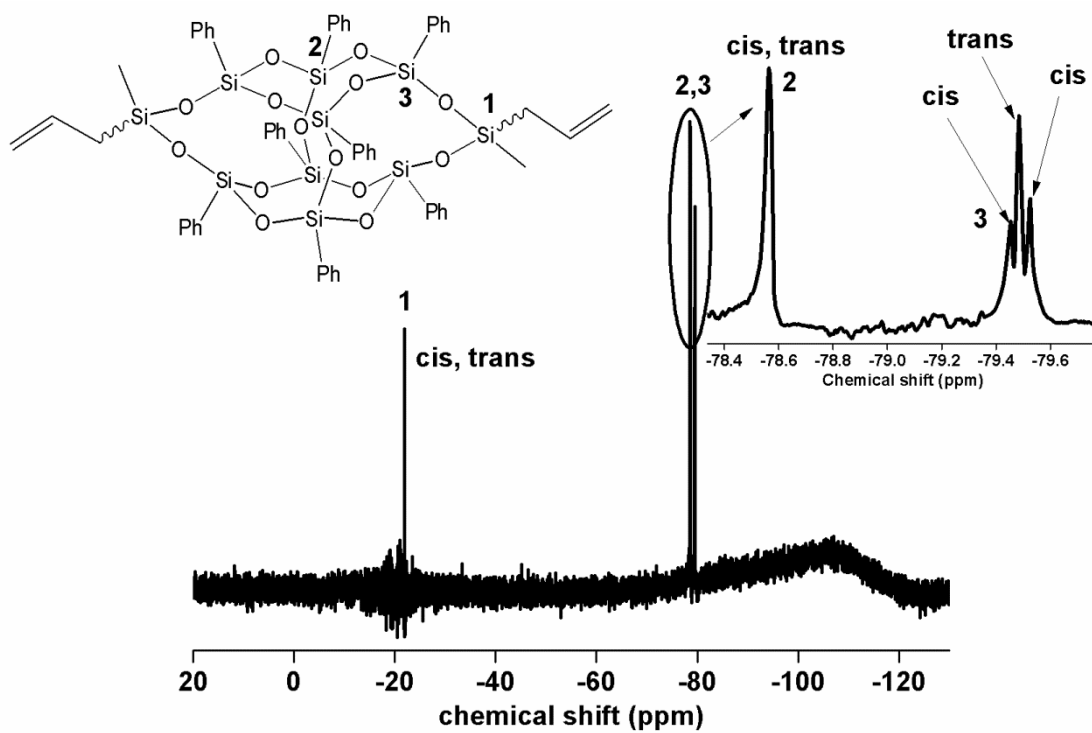


Fig. S12. The ^{29}Si NMR spectra of 3,13-di(3-propenyl)-3,13-dimethyl-1,5,7,9,11,15,17,19-octaphenylhexacyclo[15.3.1(1,13).1(3,11).1(5,17).1(9,15)]decasiloxane. (500 MHz, CDCl_3)

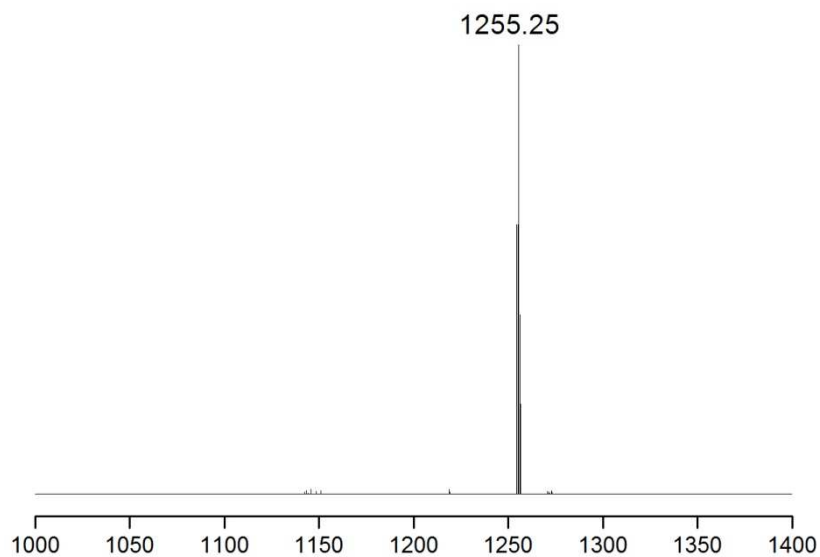


Fig. S13. MALDI-TOF MS of 3, 13-di(3-propenyl)-3,13-dimethyl-1,5,7,9,11,15,17,19-octaphenylhexacyclo[15.3.1(1,13).1(3,11).1(5,17).1(9,15)]decasiloxane.

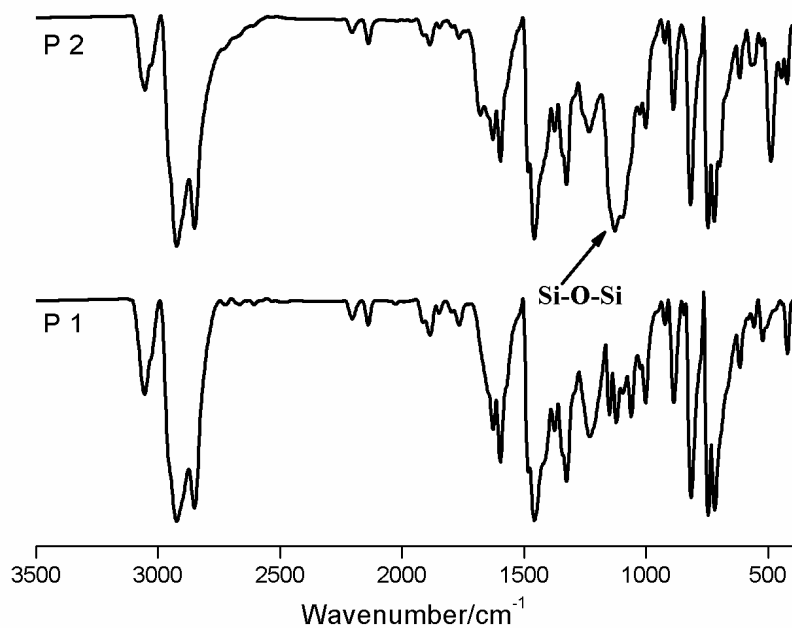


Fig. S14. The FT-IR spectra of P1 and P2.

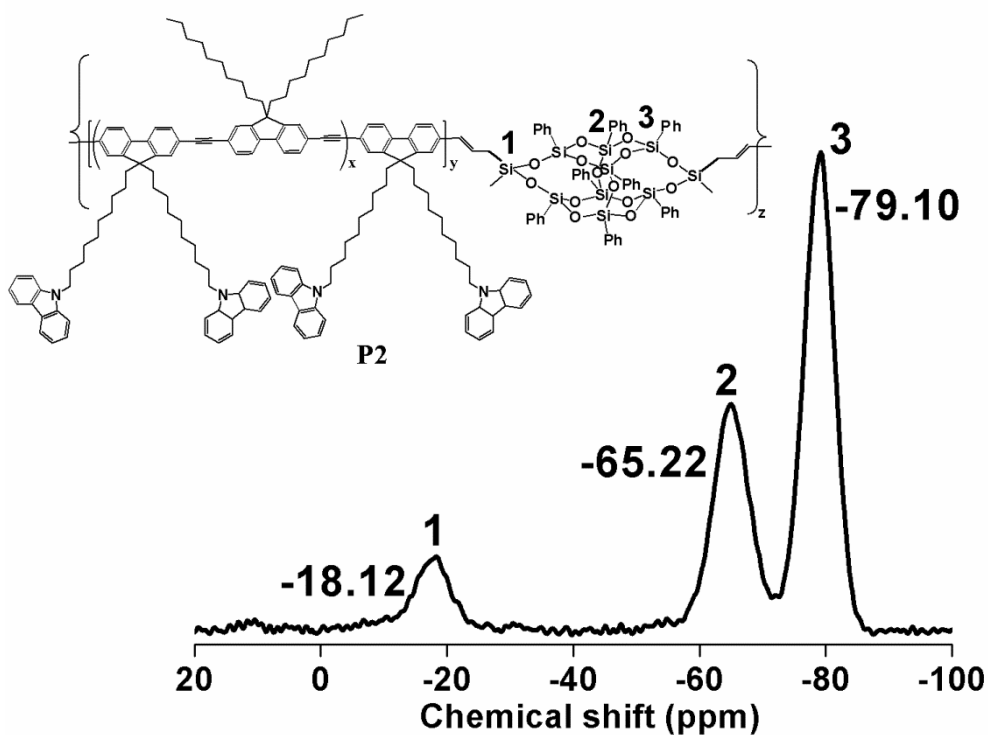


Fig. S15. The solid ²⁹Si NMR spectrum of P2.

Reference

- [1] Olmsted J. The Journal of Physical Chemistry 1979; 83: 2581–4.